Contrib Mineral Petrol (2013) 165:1087–1106
DOI 10.1007/s00410-013-0849-6

ORIGINAL PAPER

Volatiles contents, degassing and crystallisation of intermediate magmas at Volcan de Colima, Mexico, inferred from melt inclusions

Olivier Reubi · Jonathan Blundy · Nicholas R. Varley

Received: 24 March 2011 / Accepted: 3 January 2013 / Published online: 12 February 2013

Abstract In volatile-saturated magmas, degassing and crystallisation are interrelated processes which influence the eruption style. Melt inclusions provide critical information on volatile and melt evolution, but this information can be compromised significantly by post-entrapment modification of the inclusions. We assess the reliability and significance of pyroxene-hosted melt inclusion analyses to document the volatile contents (particularly H_2O) and evolution of intermediate arc magmas at Volcán de Colima, Mexico. The melt inclusions have maximal H_2O contents ($\leq$4 wt%) consistent with petrological estimates and the constraint that the magmas crystallised outside the amphibole stability field, demonstrating that pyroxene-hosted melt inclusions can preserve H_2O contents close to their entrapment values even in effusive eruptions with low effusion rates (0.6 m^3 s^{-1}). The absence of noticeable H_2O loss in some of the inclusions requires post-entrapment diffusion coefficients ($\leq 1 \times 10^{-13}$ m^2 s^{-1}) at least several order of magnitude smaller than experimentally determined H^+ diffusion coefficient in pyroxenes. The H_2O content distribution is, however, not uniform, and several peaks in the data, interpreted to result from diffusive H_2O reequilibration, are observed around 1 and 0.2 wt%. H_2O diffusive loss is also consistent with the manifest lack of correlations between H_2O and CO_2 or S contents. The absence of textural evidence supporting post-entrapment H_2O loss suggests that diffusion most likely occurred via melt channels prior to sealing of the inclusions, rather than through the host crystals. Good correlation between the melt inclusion sealing and volcano-tectonic seismic swarm depths further indicate that, taken as a whole, the melt inclusion population accurately records the pre-eruptive conditions of the magmatic system. Our data demonstrate that H_2O diffusive loss is a second-order process and that pyroxene-hosted melt inclusions can effectively record the volatile contents and decompression-induced crystallisation paths of vapour-saturated magmas.

Keywords H_2O · CO_2 · Degassing · Crystallisation · Diffusion · Volcan de Colima · Arc magmas

Communicated by G. Moore.

Electronic supplementary material The online version of this article (doi:10.1007/s00410-013-0849-6) contains supplementary material, which is available to authorized users.

O. Reubi
ETH Zurich, Institute of Geochemistry and Petrology, Zurich, Switzerland

Present Address:
O. Reubi (✉)
Inst. des sciences de la Terre, Université de Lausanne, Lausanne, Switzerland
e-mail: olivier.reubi@unil.ch

J. Blundy
School of Earth Sciences, University of Bristol, BS8 1 RJ, Bristol, UK

N. R. Varley
Facultad de Ciencias, Universidad de Colima, Colima, Mexico

Introduction

Good constraints on the volatile contents of arc magmas are essential to understand the geochemical cycles of volatile elements. Moreover, volatiles play an important role in arc magmatism by strongly influencing the processes of mantle melting, magma differentiation and eruptive style (Kelley et al. 2010; Roggensack et al. 1997; Sisson and Grove 1993; Wallace 2005). Arc volcanoes often erupt

explosively and show abrupt transitions between highly explosive Plinian eruptions to gentle effusion of lava domes accompanied by Vulcanian explosions. Identifying the processes controlling these transitions and developing predictive models is an important challenge for the volcanology community. As volcanic eruptions are driven, primarily, by loss of volatiles from ascending magma, the exsolution, expansion and migration of volatiles are key parameters in understanding eruption dynamics. The interdependence between crystallisation and degassing is an additional factor influencing magma ascent and eruption dynamics because the viscosity of magmas is strongly affected by the amount of crystals (and bubbles) and dissolved H_2O contents. Complex interplays and feedback mechanisms between the initial volatile contents of the magma and their ascent, degassing and crystallisation rates ultimately control the evolution and eruption of volatile-saturated magmas (Blundy and Cashman 2005; Melnik and Sparks 1999; Sparks 1997).

Phenocryst-hosted melt inclusions provide valuable information on the pre-eruptive volatile contents of arc magmas and on the degassing paths followed during their ascent through the upper crust (e.g. Lowenstern 2003; Roggensack 2001; Sisson and Layne 1993; Spilliaert et al. 2006; Wallace 2005). In addition, melt inclusions have been used to document the relationship between crystallisation and degassing (Blundy and Cashman 2005; Humphreys et al. 2008a; Johnson et al. 2010, 2008; Wallace et al. 1999). Inverse correlations between H_2O contents and melt crystallinity are interpreted as evidence that decompression induced both degassing and crystallisation in subvolcanic magmatic systems (Blundy and Cashman 2005). Melt inclusions, therefore, provide an excellent tool to establish the volatile contents and degassing–crystallisation relationship of magmas. Post-entrapment modifications of the melt inclusions can, however, significantly compromise the melt inclusion record. Post-entrapment crystallisation of the host mineral on the wall of the inclusion or of daughter crystals within the inclusion commonly affect melt inclusions and diffusive loss of H^+ or H_2O through the host crystal is a concern (Danyushevsky et al. 2002). When CO_2 is considered along with H_2O, melt inclusions rarely show trends that can be ascribed to simple decompression (Blundy and Cashman 2005; Humphreys et al. 2008a; Johnson et al. 2010, 2008; Wallace et al. 1999). The absence of simple relationship between H_2O and CO_2 is generally interpreted as the result of complex magma degassing histories involving fluxes of CO_2-rich vapour through an upper crustal magmatic system (Blundy et al. 2010) or cooling-induced crystallisation in vapour-saturated systems (Wallace et al. 1999). Alternatively, post-entrapment diffusive loss of H^+ or H_2O through the host crystal (Danyushevsky et al. 2002) or non-equilibrium fractionation during rapid degassing (Gonnermann and Manga 2005) may cause such dispersion. Diffusive loss of H_2O has been shown experimentally to occur on timescales of hours to days in olivine-hosted melt inclusions (Massare et al. 2002; Portnyagin et al. 2008; Lloyd et al. 2012). No experimental data exist for pyroxene-hosted melt inclusions, but the timescales obtained for olivines indubitably raises concerns about the extent of post-entrapment H_2O loss from melt inclusions in general. Careful evaluation of the reliability of the melt inclusion record, particularly the volatile contents, is necessary before making inferences about the evolution of the magmas in the subvolcanic magmatic system.

The extent to which melt inclusions effectively depict the conditions in the magmatic system prior to eruption is an additional concern. U-series disequilibria studies of phenocrysts in intermediate magmas generally indicate ages of crystal cores that pre-date eruption by hundreds to thousands of years (Cooper and Reid 2008; Reid 2003). The melt inclusions may, therefore, be expected to provide an integrated record that covers the same range of time. At Mount St Helens, time series analyses of melt inclusions in the 1980–1986 magmas do, however, show correlations with the seismic and gas flux recorded at the surface during the same period (Blundy et al. 2008). This suggests that, independently of the age of the crystals, the melt inclusions may record the conditions occurring in the system prior to the eruption. Establishing a link between the melt inclusion and the pre-eruption volcano monitoring records is essential to evaluate the significance of the melt inclusions. Conversely, if a link can be established the melt inclusions may be used to interpret the volcano monitoring signal in terms of subvolcanic magmatic processes, an enduring challenge in volcanology.

Here, we present a study of volatiles in pyroxene-hosted melt inclusions from the 1998–2005 effusive and Vulcanian eruptions at Volcán de Colima, Mexico. Our aim is to evaluate the reliability and significance of the melt inclusion record on the basis of their chemistry, as well as petrological estimates of magmatic H_2O contents. We also investigate the link with the volcano monitoring record (effusion rate and seismicity) and discuss the degassing–crystallisation relationship.

Volcán de Colima

Volcán de Colima, a nearly perfect cone rising to 3,850 m a.s.l. in western Mexico (Fig. 1), is one of the most historically active volcanoes in North America (Luhr and Carmichael 1980). The active cone of Volcán de Colima is growing inside a horseshoe-shaped caldera that formed by sector collapse of an earlier edifice 4.3 ky ago (Luhr and

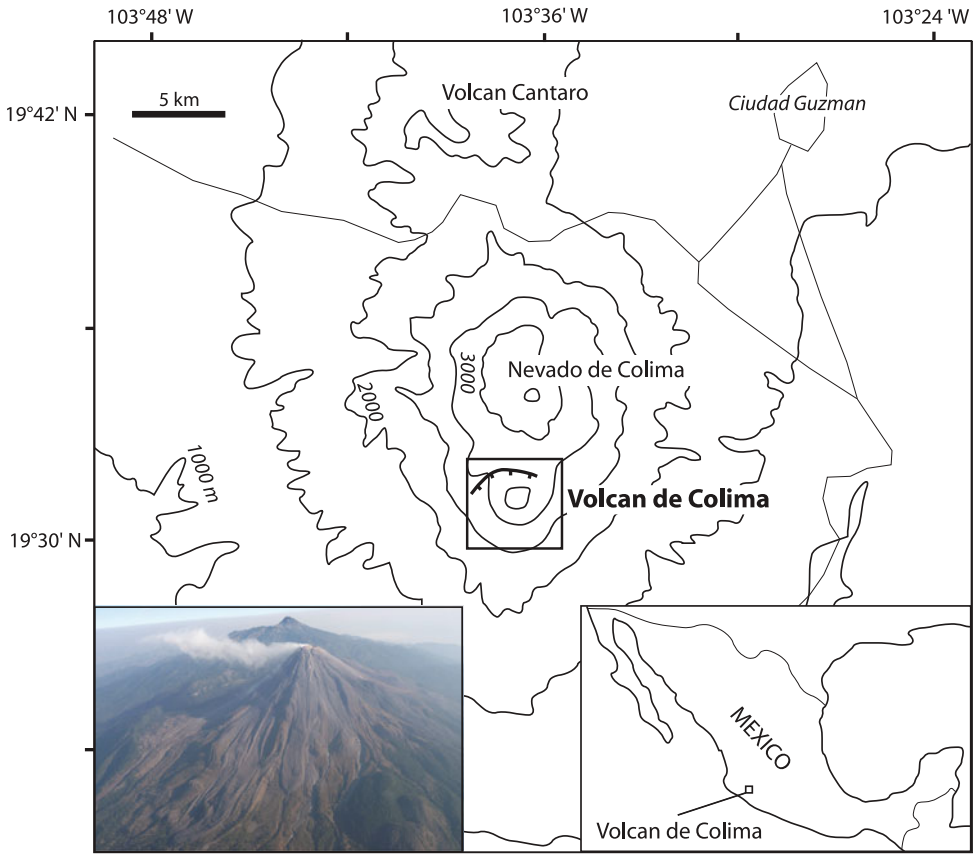

Fig. 1 Location map of Volcán de Colima. Volcán de Colima is the youngest and only active cone of a large complex edifice that encompasses 1.5 Ma of activity and includes Volcán Cántaro and Nevado de Colima. *Inset* picture shows an aerial view of Volcán de Colima taken from the south in February 2011. The 1998–1999 lava flows can be seen coming from the summit in the foreground. The peak at the back is Nevado de Colima. The caldera floor, where the Vulcanian bombs were collected (El Playón), can be seen under the steam cloud at the foot of the caldera scarp. The caldera wall is also shown on the map

Prestegaard 1988). Investigation of historical activity reports reveals a pattern of eruptive cyclicity since the early sixteenth century (Breton et al. 2002; Luhr 2002; Luhr and Carmichael 1990). Each cycle comprises an initial period of dome growth followed by intermittent eruption of lava flows, and gas and ash-to-block Vulcanian eruptions. The cycles end with cataclysmic sub-Plinian to Plinian eruptions, the most recent of which occurred in 1818 and 1913. The current eruptive cycle started in 1961 and includes effusive eruptions in 1961–1962, 1975–1976, 1981–1982, 1991 and 1998–2011. The ongoing eruption phase started in November 1998 after 7 years of repose. The activity is characterised by effusive periods of dome growth and lava flows (in 1998–1999, 2001–2003, 2004 and 2007–2011) and periods of intermittent explosive Vulcanian events. In 1999, 2003 and 2005, several major Vulcanian explosions produced eruption columns up to 11 km (a.s.l.) high and associated pyroclastic flows. These eruptive events represent the most explosive behaviour since the last Plinian eruption in 1913. This, in conjunction with an observed 80–100 years periodicity for recent Plinian eruptions at Volcán de Colima (Breton et al. 2002; Luhr and Carmichael 1990), has raised concerns amongst volcanologists about the possible imminence of a major Plinian event.

The total volume of magma erupted between 1998 and 2005 is estimated at 5.9×10^7 m^3, with 66 % of this volume erupted during late 1998—early 1999 effusive

Table 1 Volume of magma extruded and average effusion rate for the eruptive phases between 1998 and 2005 at Volcan de Colima

	November 1998–February 1999	February–July 1999	July 1999–May 2001	May 2001–March 2003	July–August 2003	September–December 2004	February–September 2005
Eruption style	Effusive	Vulcanian	Sporadic Vulcanian	Effusive	Vulcanian	Effusive	Vulcanian
Volume (m^3)	3.90E+07	2.40E+06	–	1.04E+07	?	4.70E+06	2.50E+06
Average effusion rate (m^3 s^{-1})	4.11	0.17	–	0.17		0.60	0.16

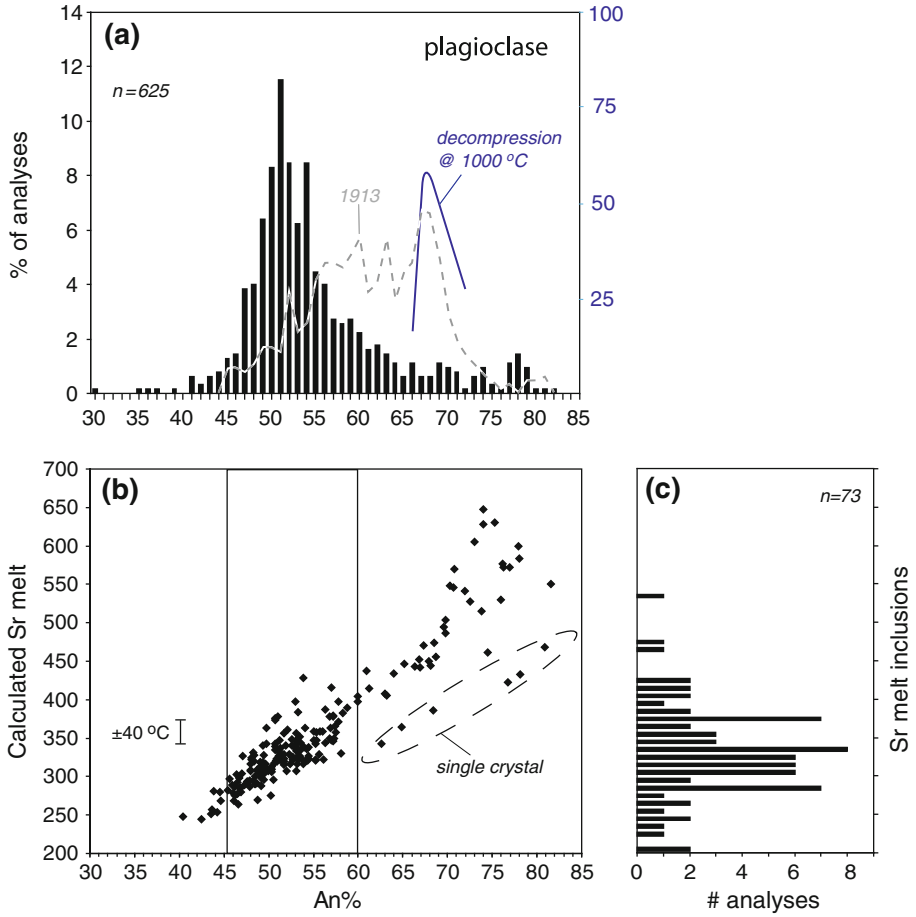

Fig. 2 Plagioclase and melt inclusion compositions. **a** Histogram showing the ranges of compositions of phenocryst-sized plagioclase in the 1998–2005 magmas (*black bars*) and 1913 magmas (*dashed line*) (Pickles, unpublished data), as well as the range of plagioclase compositions expected for decompression-induced crystallisation of hydrous andesitic melts at 1,000 °C [*solid line*, based on experimental data from Moore and Carmichael (1998)]. **b** An% of plagioclase versus Sr contents of melts determined from the plagioclase Sr concentrations using the $^{Sr}K_{D\ plag/melt}$ expression from Blundy and Wood (1991) for a temperature of 1,000 °C. The *error bar* represents the range of calculated Sr corresponding to 1,000 ± 40 °C. Amongst the 50 crystals analysed, only one (indentified by *dashed line* contours) shows data points systematically offset to higher An% at a given calculate melt Sr content compared to the others crystals analysed. This crystal most likely formed at higher PH_2O than the other plagioclases and possibly represents a residual crystal from an earlier magma with higher H_2O content, possibly the 1913 magma. **c** Histogram showing the distribution of Sr in melt inclusions

phase (Table 1). The average effusion rate for the different period of activity range from 4.1 $m^3\ s^{-1}$ for the 1998–1999 effusive phase to 0.16 $m^3\ s^{-1}$ during the 2005 Vulcanian phase (Table 1). Peak effusion rate $\leq$8 $m^3\ s^{-1}$ occurred in October 2004.

Previous work on the petrology of 1998–2005 andesites

We examined a suite of samples that cover the effusive and explosive eruptive styles since the onset of activity in 1998. Samples representative of the effusive phases were collected from the lava flows and domes. For the Vulcanian eruptions, bread-crust bombs collected on the caldera floor (El Playón) directly north of the active cone were used. The petrology and geochemistry of the samples, as well as the major and trace element chemistry of some of the melt inclusions are presented in detail in Reubi and Blundy (2008). Only a summary is given here.

All investigated magmas are andesitic in composition with 59.0–61.4 wt% SiO_2 (H_2O-free), as are all historical lavas (Luhr 2002; Luhr and Carmichael 1980, 1990; Mora et al. 2002; Reubi and Blundy 2008; Savov et al. 2008). The 1998–2005 andesites are petrographically homogenous with 30–38 % phenocryst-sized minerals (i.e. irrespective of their origin and extent of equilibrium in the erupted magma). Plagioclase is the dominant phase, followed by clinopyroxene, orthopyroxene, titanomagnetite, and rare resorbed hornblende. Phenocryst compositions are uniform and unimodal in all samples and show broad main populations An% 60–40 and Mg# 77–70 for plagioclase and pyroxenes, respectively (Figs. 2a, 3a). Ca-rich plagioclase

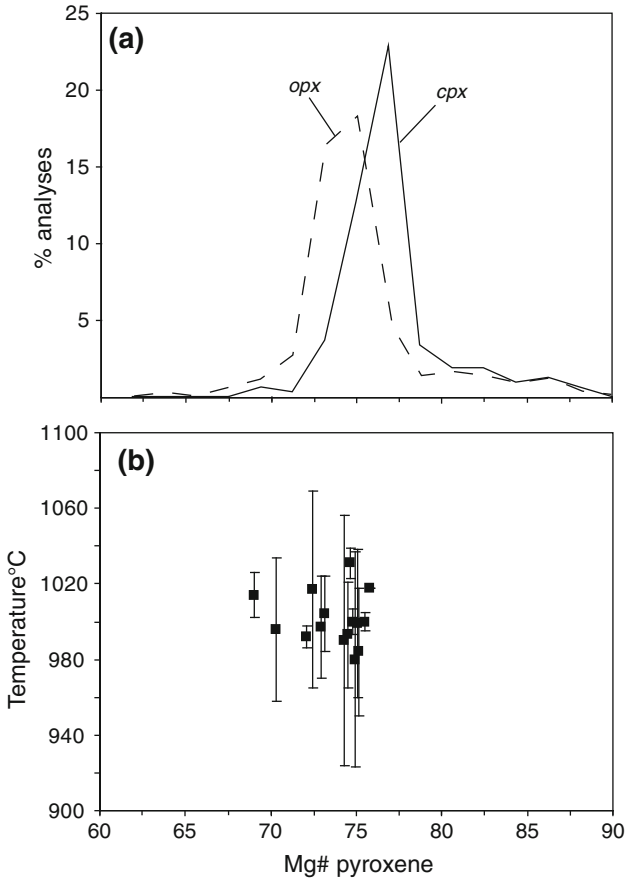

Fig. 3 Pyroxene compositions and thermometry. **a** Histogram showing the ranges of compositions of pyroxenes in the 1998–2005 magmas. **b** Mg# pyroxenes versus temperatures calculated for touching pairs according to the method of Andersen et al. (1993). Mg# shown are those for the orthopyroxenes from the pairs used in thermometry. *Error bars* are uncertainties reported by the QUILF program

(to An_{82}) and Mg-rich pyroxene (to Mg# 88) outliers are found in all lavas. Three textural types of plagioclase are observed. (1) The majority of plagioclases show oscillatory zoning with moderate variations in compositions (<10 mol% An). (2) Some crystals have a pronounced concentric resorption zone associated with moderate but sharp increase in X_{An} ($\leq$10 mol% An) from core to rim. (3) Occasional crystals with textural evidence for major resorption events are also observed. The majority of these resorbed plagioclases have corroded high-An ($\sim An_{80}$) cores filled in by low-An plagioclase ($An_{55–45}$) and melt inclusions, forming a patchy texture on BSE images. These resorbed high-An plagioclases have oscillatory-zoned rims with the same range of X_{An} as the oscillatory phenocrysts lacking An-rich cores. The presence of gabbroic crystal clots, up to few mm in size, and showing a range of textures from glomerocrysts with vesiculated interstitial glass to plutonic, is a ubiquitous feature of these andesites and indicates that mingling between silicic melts and partially consolidated plutonic rocks exercised an important influence on bulk rock compositional trends and variability (Reubi and Blundy 2008). Detailed point counting using BSE images indicates that the gabbroic clots represent 5–15 % of the total volume, the mafic crystals from disaggregation of the clots 3–10 % and the weakly zoned crystals inferred to be true phenocrysts 23–25 %, with an average of 20 % plagioclase, 2.8 % orthopyroxene, 0.7 % clinopyroxene and 0.5 % titanomagnetite.

Temperatures calculated for touching orthopyroxene and clinopyroxene pairs with Mg# 76–69 range from 980 to 1,030 °C (average 1,000 °C) according to the method of Andersen et al. (1993) (Fig. 3b) (Luhr 2002; Reubi and Blundy 2008; Savov et al. 2008). Touching ilmenite-magnetite pairs ($n = 3$) give temperatures of 993–938 °C and log (fO_2) values of −9.2 to −9.96 using the method of Ghiorso and Evans (2008) (Reubi and Blundy 2008). On account of their relatively rapid reequilibration, the lowest Fe–Ti oxides temperatures are likely to provide an estimate of pre-eruptive temperature, whereas the two pyroxenes and highest Fe–Ti oxides temperatures record temperatures of crystallisation.

Melt inclusions show a broad range of compositions and can be divided into two distinct chemical groups on the basis of their K_2O contents: termed “low-K” and “high-K” by (Reubi and Blundy 2008). The high-K melt inclusions have high large ion lithophile element (LILE) signatures that are clearly distinct from the bulk composition of the magmas and are thought to have formed by partial melting of plutonic fragments and crystal cumulates during their assimilation into a silicic melt. These high-K melt inclusions have limited significance regarding the evolution of the melt feeding Volcán de Colima and are not discussed further. Detailed investigation of the chemistry of low-K melt inclusions demonstrates that they effectively record the composition of the crystallising melt and their major element chemistry was not modified appreciably by post-entrapment crystallisation processes (exception of H_2O, see below). This group of inclusions can, therefore, be considered as representative of the evolution of the volumetrically dominant melt component in the system prior to eruption and are used here to probe the relationship between degassing and crystallisation.

Analytical techniques

Melt inclusions hosted in clinopyroxene and orthopyroxene were analysed. Individual phenocrysts were mounted in Epoxy resin and polished to expose the melt inclusions. Each mount was examined using back-scattered electron (BSE) images and under a microscope to ascertain the

absence of visible daughter crystals and bubbles in the inclusions. The melt inclusions were first analysed by electron-microprobe (EMP) for major and minor elements and subsequently analysed for H_2O, CO_2 and trace elements by secondary ion mass spectrometry (SIMS). After SIMS analyses, the melt inclusions were reanalysed for S, Cl and F by EMP using a high beam current to improve precision.

Melt inclusions, groundmass glasses and plagioclases were analysed at the University of Bristol using a CAMECA SX-100 five-spectrometer WDS instrument and at ETH Zurich using a JEOL JXA-8200. Glasses and plagioclase were analysed using 20 kV accelerating voltage, 2 nA beam current and 12–15 μm beam diameter, with Na and Si analysed first to reduce the effects of alkali migration (Humphreys et al. 2006). S, Cl and F were analysed using a 20 kV accelerating voltage, 30 nA beam and for 120 s counting time. The effect of alkali loss and associated beam damage to the glass at these conditions was monitored by successive analyses of the same spot on a glass standard and found to have a negligible effect on S, Cl and F. Pyrrhotite, FeS, was used as standard for S analyses and the SKα peak was measured using a PETH crystal, which has lower wavelength resolution, to minimise the impact of the peak shift related to the oxidation state of S.

The concentrations of H_2O and CO_2 were measured by ion-microprobes at the University of Edinburgh. H_2O was measured using a Cameca IMS-4f instrument following the procedure described in Blundy et al. (2008, 2010). A 15 keV impact energy primary beam of O^- ions was used to generate positive secondary ions, which were then accelerated to 4,500 eV, with an offset of −75 eV (±20 eV) to reduce transfer of molecular ions into the secondary column. ^1H was analysed using 6 nA current at the sample surface, corresponding to a ~15 μm sputter area. The first 7 cycles of each analysis were disregarded, in order to minimise any surface contamination and the top surface damaged by electron-beam irradiation during EMP analyses (~1 μm at the EMP analytical conditions described above, Humphreys et al. 2006). The final 8 cycles were used to process the data. CO_2 was measured using a Cameca 1,270 ion-microprobe. A 22 keV impact energy primary beam of 4nA $^{16}O_2^-$ was used, and positive secondary ions were extracted at 10 keV, with an energy offset of 50 eV. Measurements were done at sufficient resolution to fully resolve $^{24}Mg^{2+}$ from $^{12}C^+$. Note that this procedure eliminates the large corrections required for $^{24}Mg^{2+}$ when using lower mass resolution (Blundy et al. 2008). Thirty cycles were measured and the final 10 used to process the data. For both H_2O and CO_2 measurements, counts were normalised to ^{30}Si and the analyses were calibrated against a set of rhyolite glass standards of known H_2O (0.29–4.1 wt%) and CO_2 (29–2,860 ppm). Inclusion-free quartzes from the Taupo Volcanic Zone inserted in each grain mount were used to measure the instrumental blank for H_2O and CO_2. Minimum detection limits, defined as three standard deviations of the mean blank in each sample mount, were between 40 and 230 ppm H_2O and 12 and 28 ppm CO_2, depending on sample. Typical standard errors, based on propagated counting statistics, are 5 % relative for H_2O and 6 % relative for CO_2.

Trace element analyses in glasses and plagioclases were carried out using the Cameca IMS-4f instrument at the University of Edinburgh with 10 kV (nominal) O^- primary beam and 4.5 kV positive secondary ions following the procedures described in Reubi and Blundy (2008). Trace element calibration was carried out using NIST SRM610 multi-elements glass. For Sr analyses in plagioclase, the calibration was corrected for the ion yield of NIST SRM610 relative to Lake County plagioclase using ratios determined by R. Hinton (personal communication). Typical uncertainties, based on counting statistics, are 8 % relative.

Results

The complete melt inclusion, groundmass glasses and plagioclase dataset is presented in electronic supplementary data. The melt inclusion data includes new major, trace and volatile elements analysis for 40 melt inclusions, as well as H_2O and S contents of melt inclusions for which the major and trace elements contents were presented in Reubi and Blundy (2008).

Melt inclusions compositions and volatile contents

The low-K melt inclusions have between 64.2 and 75.8 wt% SiO_2 (H_2O-free). For most major elements, the compositional trends exhibited by the melt inclusions extend to the groundmass glass compositions (Fig. 4). With increasing SiO_2 contents, CaO, MgO, FeO, Al_2O_3 and NaO decrease and K_2O increases. FeO and TiO_2 are not correlated in the melt inclusions, in contrast to the groundmass glasses that exhibit a fairly linear trend (Fig. 4d). There is no distinction between the chemical compositions of melt inclusions in clinopyroxenes and orthopyroxenes. The compositional range remains essentially constant for magmas erupted between 1998 and 2005. Groundmass glasses have the most evolved compositions with a SiO_2 (anhydrous) range from 71.3 to 78.0 (Fig. 4). They form elongated trends that overlap and extend the trends defined by the most evolved low-K melt inclusions, except for FeO and TiO_2 (Fig. 4d).

Melt inclusions in the 1998–2005 magmas have low H_2O contents (≤4.1 wt%) (Fig. 5) compared to others

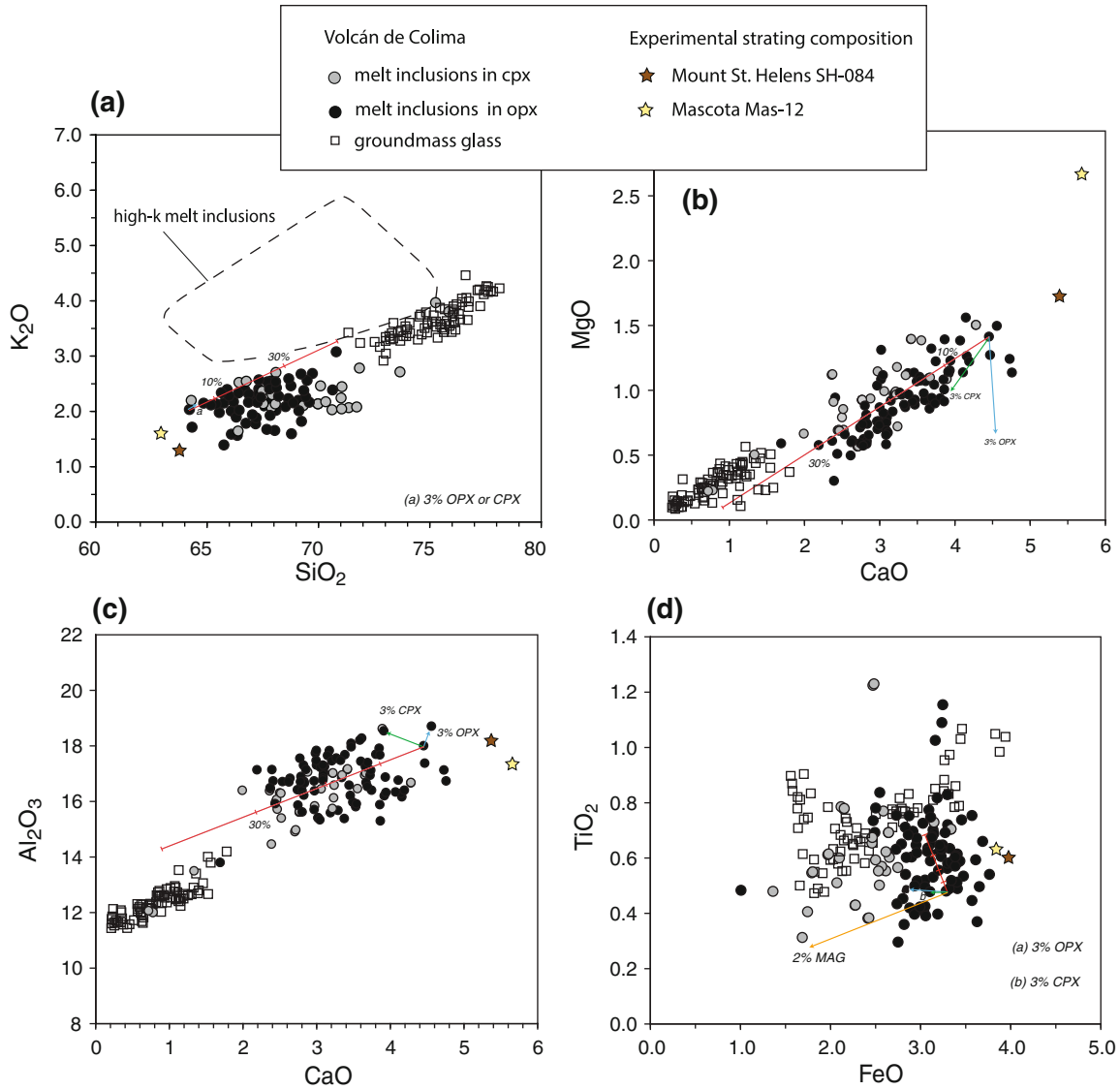

Fig. 4 Major element variation diagrams for the melt inclusions and groundmass glasses in Volcán de Colima 1998–2005 andesites. Major elements are from EMP analyses (data from Reubi and Blundy 2008). The *dashed field* shows the compositions of high-K melt inclusions present in these magmas and interpreted as exotic melts thought to be formed by partial melting of plutonic fragments and crystal cumulates during assimilation in the silicic melt characterise by the others (low-K) melt inclusions (Reubi and Blundy 2008). The *small vectors* show the effect of 3 % crystallisation of clinopyroxene (*green vector*) and orthopyroxene (*blue vector*). The *red line* shows the crystallisation trend produced by fractionation of the phenocrysts proportion estimated on the basis of point counting of BSE images (20 % plagioclase, 2.8 % orthopyroxene, 0.7 % clinopyroxene and 0.5 % titanomagnetite). The *stars* show the composition of the starting materials used in the experiments shown in Fig. 12. Mascota experimental data are from Moore and Carmichael (1998). Mount St Helens data are from Rutherford et al. (1985)

andesitic arc volcanoes that commonly show maximum values between 4 and 6 wt% (Wallace 2005). The range of H_2O contents in individual sample differ significantly with variations between 0.11 and 3.5 wt% H_2O. The overall distribution of 81 analyses shows peaks around 0.2 and 0.8–1 wt% (Fig. 5). No systematic difference is observed between the effusive and explosive eruptions, although one of the vulcanian eruptions has a larger range of H_2O contents extending to 4.1 wt%. The H_2O contents of the 1998–2005 melt inclusions are lower than the concentrations measured in melt inclusions from the 1913 Plinian eruption that range from 2.8 to 6.2 wt% H_2O (Atlas et al. 2006; Luhr 2006).

The CO_2 contents of the 1998–2005 melt inclusions range from 236 ppm to below detection limit (<12–28 ppm) (Fig. 6). CO_2 does not vary systematically with H_2O, but the highest contents are found in inclusions with high H_2O contents (Fig. 6). Entrapment pressures calculated using the solubility model of Papale et al. (2006) range from 160 to 3 MPa at 1,000 °C, the average

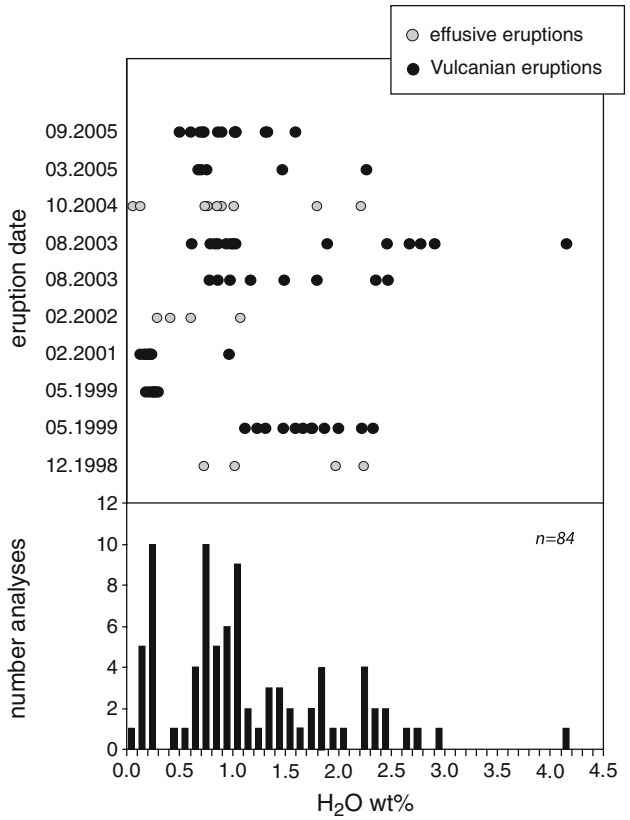

Fig. 5 H_2O contents of melt inclusions in Volcán de Colima 1998–2005 magmas. *Upper panel* Range of melt inclusion H_2O contents in individual eruptions including both effusive and explosive samples. *Lower panel* Histogram showing the distribution of H_2O in the complete population

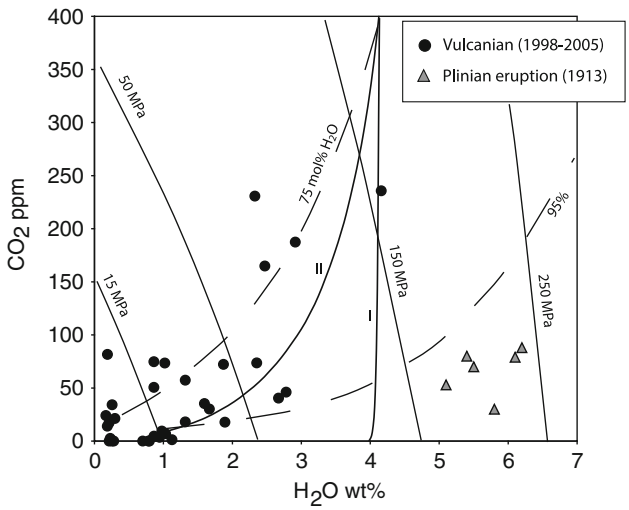

Fig. 6 Volatile contents of melt inclusions from Volcán de Colima. Vapour isopleths (*long dash lines*) and isobars (*continuous lines*) are calculated using the solubility model of Papale et al. (2006) for the average melt inclusion composition. *Thick curves I* and *II* represent the degassing path of magmas for open-system and closed-system with 2 % excess vapour degassing, respectively, for an initial magma with 4.15 wt% H_2O and 400 ppm CO_2. These degassing paths are calculated using Newman and Lowenstern (2002) for a rhyolitic melt at 1,000 °C. Melt inclusion data for the 1913 Plinian eruption are from Luhr (2006)

temperature obtained from two-pyroxene thermometry, and assuming Fe_2O_3/FeO ratios in the melt calculated using the formulation of Kress and Carmichael (1991) for a log (fO_2) value of −9.3. The 1913 inclusions have low CO_2 contents (30–88 ppm) despite their high H_2O contents (Luhr 2006), corresponding to higher calculated entrapment pressures of 160–240 MPa (Fig. 6). S (<1,300 ppm) shows no correlation with H_2O and a weak correlation with CO_2 (Fig. 7a, b). There is a particularly large range of S values at intermediate H_2O contents (Fig. 7a). Cl contents range from 1,540 to 2,600 ppm. There is no correlation with H_2O but there is a weak negative correlation with CO_2 (Fig. 7c). As observed for H_2O, there are no systematic variations in S and Cl contents between explosive and effusive eruptions, but the melt inclusions from effusive eruptions tend to have lower H_2O contents at a given S content (Fig. 7a).

Sr concentrations were measured for a subset of plagioclases by ion probe. The plagioclases and the position of the analyses within the crystals were selected on the basis of BSE images to cover the range of An% and textural types of plagioclase observed in each sample. The plagioclases analysed vary in composition from An_{40} to An_{81} (Fig. 2b), with 80 % of them in the range An_{40-60}. These compositional range and distribution are similar to those shown by the complete plagioclase dataset shown in Fig. 2a. Sr contents range from 768 to 1,398 ppm.

Discussion

Before using the melt inclusion data to document the degassing and crystallisation paths of the magmas and making inferences about the magmatic system, it is essential to assess the extent of post-entrapment modifications. To this end, we first discuss the textural and chemical characteristics of the inclusions. To further evaluate the reliability of the melt inclusion H_2O contents, independent estimates of the melt H_2O contents are then obtained from petrology of the magmas. The significance and temporal representativeness of the melt inclusion record is then discussed in the light of experimental petrology and volcano monitoring data.

Reliability of the melt inclusions

Textural and chemical indications of post-entrapment modification of melt inclusions

Post-entrapment crystallisation of the host mineral on the wall of the inclusion or of daughter crystals within the

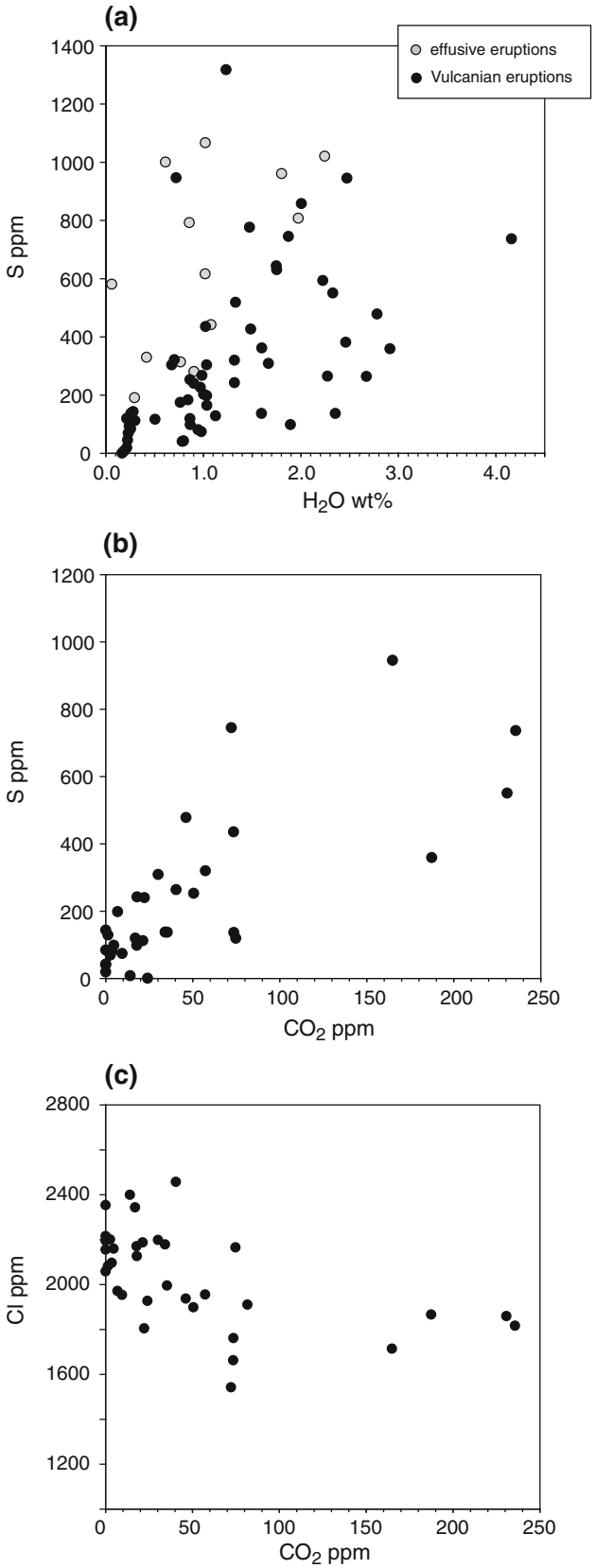

◀**Fig. 7** Volatile element variation diagrams for the melt inclusions in the 1998–2005 andesites. **a** S versus H_2O. **b** S versus CO_2. **c** Cl versus CO_2. Low H_2O contents of some of the inclusion with moderate to high S contents may indicate H_2O loss by diffusion trough the host crystal

inclusion is known to affect melt inclusion chemistry (Danyushevsky et al. 2002). Although these features can be observed in some Volcán de Colima melt inclusions, only inclusions that are glassy and free of visible daughter crystals and bubbles have been analysed in this study. Small shrinkage bubbles or daughter crystals may, nonetheless, have been ground away during sample preparation or may be hidden from the plane of view. When a daughter mineral is observed, it consists generally of a single small (1–2 μm) titanomagnetite crystal. The similar compositional ranges shown by the clinopyroxenes-hosted and orthopyroxenes-hosted melt inclusions indicate that the amount of post-entrapment crystallisation of the host phase on the wall of the inclusion did not exceed 2 % (Fig. 4). The primary compositional trends exhibited by the melt inclusions are consistent with up to 30 % crystallisation of the phenocryst assemblage estimated on the basis of BSE images (i.e. 83 % plagioclase, 12 % orthopyroxene, 3.2 % clinopyroxene and 1.1 % titanomagnetite), except for FeO and TiO_2. The amount of post-entrapment crystallisation is, therefore, small compared to the overall crystallisation trend recorded. The absence of any trend for FeO and TiO_2 most likely results from post-entrapment crystallisation of small amounts (<2 %) of titanomagnetite (Fig. 4d), suggesting that small daughter titanomagnetite crystal was effectively ground away or were hidden from the plane of view in some of the analysed melt inclusions.

The scatter in melt inclusion H_2O and CO_2 contents shown in Fig. 6 is a common feature of arc magmas (Atlas et al. 2006; Blundy et al. 2010; Johnson et al. 2008; Schmitt 2001). Although this diversity in H_2O and CO_2 concentrations is generally interpreted as the result of complex magma degassing histories, post-entrapment diffusive loss of H^+ or H_2O through the host crystal (Danyushevsky et al. 2002; Hauri 2002; Portnyagin et al. 2008) can also cause such dispersion. Significant diffusive loss of H_2O has been shown experimentally to result in the formation of shrinkage vapour bubbles (Severs et al. 2007) and is expected to cause crystallisation of daughter crystals or decrepitation within the inclusion (Danyushevsky et al. 2002). As mentioned above, these features can be observed in some Volcán de Colima melt inclusions, but such inclusions were not analysed in this study. As for the daughter crystals, however, small shrinkage bubbles may, nonetheless, have been ground away during sample prep-

aration or may be hidden from the plane of view. In the case of unobserved shrinkage bubbles, the measured CO_2 values would represent minimum values as CO_2 partitions preferentially into the shrinkage bubble because of its low solubility compared to H_2O. Note that this process cannot account for CO_2 contents that are higher than expected during open- or closed-system degassing. This is in contrast to diffusive loss of H^+, which can displace the melt inclusions away from the degassing trends, giving an illusion of high CO_2 at a given H_2O, as clearly seen in Fig. 6. An alternative possibility is that moderate CO_2 contents in melt inclusions with low H_2O contents are the result of submicron CO_2-rich bubbles not detected during petrographic observation of the inclusions, but sputtered during SIMS analysis. Monitoring of ^{12}C counts over the course of individual ion-microprobe analyses indicates, however, that CO_2 concentrations are homogenous in the glasses, precluding the presence of micro-bubbles. It has also been shown that melt inclusions in slowly cooled lava flows are more prone to diffusive loss of H_2O than inclusions in rapidly solidified volcanic bombs (Hauri 2002; Portnyagin et al. 2008; Lloyd et al. 2012). At Colima, pristine glassy inclusions are much less common in samples from effusive eruptions than in samples from Vulcanian eruptions. This likely results from lower cooling rates in the first case, but could also indicate enhanced diffusive loss of H_2O. However, we see no systematic difference in H_2O contents in glassy inclusions in lava flows and bread-crust bombs formed during Vulcanian eruptions (Fig. 5), indicating the absence of H_2O loss during emplacement and cooling of the flows. Fe oxidation resulting from H_2O dissociation and diffusive loss of H^+ may be accompanied by precipitation of magnetite (Danyushevsky et al. 2002). The common occurrence of a small daughter crystal of magnetite in Colima inclusions is the only tangible indication that H diffusive loss may have occurred.

We conclude that small amounts of post-entrapment crystallisation affected the melt inclusions but this has limited influence on the overall chemical trends that are representative of the crystallisation trends of the magmas. In addition, there are no textural evidences indicative of diffusive loss of H_2O, except perhaps for the small daughter titanomagnetite crystals. To further assess the reliability of the melt inclusion H_2O contents, independent estimates were obtained from the petrology.

Petrological estimates of melt H_2O contents: plagioclase-melt hygrometers

Information on the H_2O contents of the crystallising melts may be obtained using plagioclase-melt hygrometers (Lange et al. 2009; Putirka 2005, 2008). These hygrometers require good constraints on the crystallisation temperature and the composition of the crystallising melt. In principle, melt inclusions in plagioclase can be used to establish with relative confidence the composition of plagioclase and melt that were in equilibrium at the time of crystallisation. At Colima, melt inclusions in the predominant oscillatory-zoned plagioclase are rare and small. The large (>20 μm) inclusions are found in resorbed crystals and are associated with a sharp increase in X_{An} or corroded high-An cores. These melt inclusions have "exotic" high-K compositions that are thought to be produced by partial melting of crystal cumulates (Reubi and Blundy 2008), suggesting that the resorbed inclusion-bearing crystals are antecrysts entrained from cumulates. Moreover, the high-K melt inclusions are not in chemical equilibrium with the predominant oscillatory-zoned plagioclases (Reubi and Blundy 2008). Consequently, these inclusions cannot be used to estimate the composition of the dominant crystallising melt. The population of plagioclase required to account for the crystallisation trends shown by the low-K melt inclusions (Fig. 4) can reasonably be assumed to be represented by the predominant oscillatory-zoned (and inclusion-free) plagioclases. To evaluate the composition of the melts in which the oscillatory-zoned plagioclases crystallised, the Sr content in the melts in equilibrium with the plagioclases were calculated on the basis of Sr concentrations measured in Colima plagioclase by ion-microprobe and the $^{Sr}K_{D\ plag/melt}$ from Blundy and Wood (1991) for a temperature of 1,000 °C. The calculated melt Sr contents overlap the Sr contents measured in the low-K melt inclusions (Fig. 2), indicating that the oscillatory-zoned plagioclases are in equilibrium with melts represented by the low-K melt inclusions in pyroxenes, as assumed above. The plagioclase An% show a positive correlation with the calculated melt Sr contents (Fig. 2b). We used this correlation to match the Sr content of the melt inclusions in pyroxenes to the range of plagioclase compositions that possibly crystallised in equilibrium with the melt represented by each inclusion. The hygrometer models H of Putirka (2005) and of Lange et al. (2009) were then used to calculate the melt H_2O content range corresponding to each melt inclusion. Irrespective of the hygrometer used, H_2O contents around 3 wt% are obtained for the least differentiated (highest MgO) melts which overlaps, within error, with the H_2O contents measured by ion probe in these inclusions (Fig. 8). Significant discrepancies are, however, observed for the most differentiated (lowest MgO) melts. The Putirka (2005) hygrometer yields a trend of decreasing H_2O with increasing degree of differentiation similar to that shown by the melt inclusions (Fig. 8a) and consistent with crystallisation driven by degassing. Conversely, the Lange et al. (2009) model yields grossly the opposite trend (Fig. 8b). Similar discrepancies between H_2O contents measured in melt inclusions and estimated using the Lange hygrometer

have previously been reported for Mount Hood andesites by Koleszar et al. (2012). As at Colima, the offset increases as the measured H_2O contents decrease and reaches up to 4 wt% for inclusions with <1 wt% H_2O. Koleszar et al. (2012) interpreted the offset as the result of H_2O loss from the melt inclusions. Mollo et al. (2011) have, however, shown that the Lange et al. (2009) hygrometer significantly overestimates the H_2O content of anhydrous melts (by 3–3.5 wt%). The discrepancies between the two hygrometers and the melt inclusions may, therefore, reflect the calibration of the Lange et al. (2009) hygrometer for intermediate melt compositions with low H_2O contents. In the Colima case, we present in the following sections evidence that degassing and crystallisation occurred concomitantly. It is unlikely that the H_2O contents of the melt increased during differentiation and that H_2O was systematically lost from the differentiated melt inclusions but not from the least differentiated ones. Moreover, the most differentiated melt inclusions have major element compositions similar to groundmass glasses (Fig. 4), which are demonstrably the products of shallow crystallisation. We, consequently, favour the results from the Putirka (2005) hygrometer model, but stress that both models indicate that the maximal H_2O contents of the crystallising melt did not significantly exceed the melt inclusion maximal values. Large uncertainties are inherent in this approach because of its reliance on the $^{Sr}K_{D\ plag/melt}$, two-pyroxene thermometry and the hygrometers calibration for low H_2O silicic melts. The results obtained provide, nonetheless, indications that the inclusions provide a reliable record of the H_2O contents of the crystallising melts when the complete population is considered and that post-entrapment diffusive loss of H_2O is a second-order process.

Processes and timescales of H_2O loss from melt inclusions

In the previous sections, we demonstrated that, when the entire population is considered, the melt inclusions provide reliable indications of the H_2O contents of the crystallising melts. The melt inclusions that form the peaks observed around 0.2 and 0.8–1 wt% H_2O (Fig. 5) are, nevertheless, on the lower end of the hygrometer H_2O range at a given MgO content and show near constant H_2O over a range of MgO contents up to 1,1 wt% (Fig. 8a), suggesting that some of these inclusions may have lost H_2O. In addition, two samples almost exclusively have melt inclusions with ~0.2 wt% H_2O (May 1999 sample Mx55 and February 2001 sample 220201) (Fig. 5). Both samples have plagioclase phenocryst compositions similar to other 1998–2005 magmas and the Putirka (2005) plagioclase-melt hygrometer gives much higher H_2O contents (1.2–2.3 wt%) for these samples. The melt inclusions apparently failed to record the H_2O contents of the crystallising melts in these

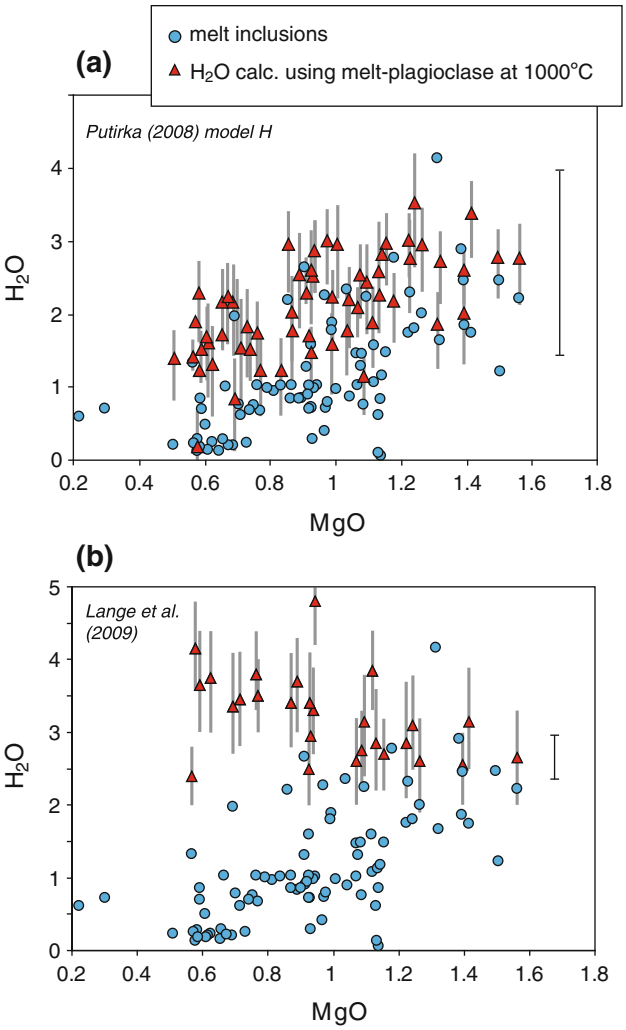

Fig. 8 H_2O contents of melts estimated on the basis of plagioclase-melt hydrometers and measured in melt inclusions versus MgO content of the melt inclusions. H_2O contents calculations were done using the hygrometer model H of Putirka (2008) **a** and Lange et al. (2009) **b**. Plagioclase-melt pairs were established on the basis of the Sr contents of melts derived from plagioclase Sr concentrations using the $^{Sr}K_{D\ plag/melt}$ expression from Blundy and Wood (1991) and the Sr concentrations of the melt inclusions using the Sr–An% relationship shown in Fig. 2. Each melt inclusion Sr content corresponds to a range of plagioclase An% (Fig. 2). Consequently, minimal and maximal values were calculated for each melt composition. The *red triangles* are average values calculated for a temperature of 1,000 °C. The *vertical grey bars* show the range between the max. values at 980 °C and the min. values at 1,030 °C for each pair. *Error bars* for calculated H_2O contents are standard errors reported for the hygrometers by Putirka (2005) and Lange et al. (2009), respectively. Three of the 60 H_2O values calculated using the Putirka model lay below zero and were discarded

cases. Some of the ~0.2 wt% H_2O inclusions have CO_2 and S contents below detection limits indicating that they have lost most of their original volatile budget. This is probably due to rupturing of the inclusions during eruption. Alternatively, this could indicate that some of the

inclusions are open and remained connected to the matrix glass through melt channels hidden from the plane of view or ground away during sample preparation, as proposed for melt inclusions from Mount St. Helens by Blundy and Cashman (2005). Other melt inclusions contain up to 80 ppm CO_2 and 581 ppm S and have CO_2 contents that are higher than expected for either open- or closed-system degassing (Figs. 6, 7a), indicating preferential loss of H_2O. Similarly, some melt inclusions from the 0.8–1 wt% H_2O peaks have CO_2 values below detection limit and low S contents (<100 ppm) probably reflecting rupturing or open inclusions and reequilibration of the volatiles at low pressure. Others have moderate to high CO_2 and S contents (up to 75–1,070 ppm, respectively) pointing towards H_2O loss.

Preferential H_2O loss may be ascribed to three distinct processes; (1) diffusive reequilibration of H_2O through the host crystal, (2) non-equilibrium degassing and (3) CO_2 fluxing. This last process calls upon equilibration of shallow stored magmas with CO_2-rich vapour percolating through the system, leading to isobaric dehydration (Blundy et al. 2010; Collins et al. 2009; Johnson et al. 2008; Rust et al. 2004; Spilliaert et al. 2006). The melts are, in this case, expected to cluster along isopleths (rather than degassing trajectories) on H_2O–CO_2 plots and show a relatively continuous range of H_2O and CO_2 contents. This is in contrast to the observed H_2O peaks and constant maximal CO_2 contents in melt inclusions with <2 wt% H_2O (Figs. 5, 6). CO_2 fluxing, therefore, is unlikely to predominate at Colima. Due to the lower diffusivity of CO_2 relative to H_2O in silicate melts, rapid degassing may result in non-equilibrium fractionation and CO_2 concentrations above equilibrium during magma ascent (Gonnermann and Manga 2005). Petrographic observations show that during formation, the melt inclusions often remain connected to the surrounding melts through small necks or tubes (Blundy and Cashman, 2005; Humphreys et al. 2008a; Bouvet de Maisonneuve et al. 2012). H_2O content gradients have been measured along tube melt inclusions not completely sealed off from the matrix glasses from the 1980 Plinian eruption of Mount St Helens (Humphreys et al. 2008b), demonstrating that diffusion of H_2O occurs in the melt channels during ascent and degassing. Non-equilibrium fractionation of volatiles will be preserved if the necks or tubes become sealed during ascent and this may explain the moderate CO_2 (and S) values in the inclusions with low H_2O contents. Finally, H_2O diffusive reequilibration through the host crystal has been shown experimentally to occur on timescales of hours to days in olivine-hosted melt inclusions (Massare et al. 2002; Portnyagin et al. 2008). No experimental data exist for pyroxene-hosted melt inclusions. However, mathematical models indicate that diffusive reequilibration of melt inclusions depends on the inclusion to host mineral radius ratio, the H_2O diffusivity in the host mineral and the H_2O mineral-melt partition coefficient (Qin et al. 1992). The diffusion coefficient of molecular water in pyroxene and olivine is poorly known, but diffusivities of H^+ are similar in these minerals (Hercule and Ingrin 1999; Woods et al. 2000), whereas the mineral-melt partition coefficients for H_2O are an order of magnitude higher for low Al pyroxenes than for olivine (Massare et al. 2002; O'Leary et al. 2010). As a result, H_2O diffusive reequilibration would be expected to be faster for pyroxene-hosted than for olivine-hosted melt inclusions. In view of the slow effusion rates of the eruptions considered here (Table 1), diffusive reequilibration may be anticipated.

Irrespective of what process resulted in H_2O loss, the most striking feature of the data is not that some inclusions lost some or all H_2O, but rather that others did not despite the low effusion rates of the eruptions considered. The time taken by the magmas to ascend to the surface can be estimated from the effusion rates and the depths of melt inclusion entrapment calculated from the pressure of entrapment of the inclusions converted to depth according to the method of (Pinel and Jaupart 2000). The maximum pressure recorded by the melt inclusions for the 1998–1999 effusive activity corresponds to a depth of 5.4 km (below the summit level). Assuming a 5.4-km-long vertical cylinder, the volume of magma erupted during this period (3.9×10^7 m^3, Table 1) requires a 48 m radius. Considering that the average effusion rate for this period of activity is 4.1 m^3 s^{-1} (table 1), a batch of magma (and its melt inclusion-bearing crystals) would take 2650 h to ascend to the surface (Fig. 9) (ascent rate = 0.0005 ms^{-1}). This is a maximum time, as the conduit between the top of the reservoir and the surface is likely to be smaller. On the basis of the hornblende reaction rim widths, Luhr (2002) estimated ascent rates in the order 0.007–0.008 ms^{-1} for the 1998 magmas, equivalent to ascent times between 187 and 214 h and a conduit with a 12–14 m radius. At the other end of the spectrum, the 2005 magmas with the lowest effusion rate (0.16 m^3 s^{-1}) would take 1570 h for a 12 m in radius conduit.

The times for H_2O diffusive reequilibration through the host crystal were calculated using the formulation of Qin et al. (1992). This model assumes spherical melt inclusions situated at the centre of spherical crystals and depends on the ratio of the inclusion and crystal radii. This simple geometry is never observed for Colima pyroxene-hosted melt inclusions. As an approximation, we used the ratio of the inclusion radius divided by the shortest distance between the centre of the inclusion and the crystal rim ($\sim$0.1 on average). H_2O mineral-melt partition coefficient values 0.01, appropriate for low Al orthopyroxene and clinopyroxenes (O'Leary et al. 2010), were used. Experimentally determined H^+ diffusion coefficients in

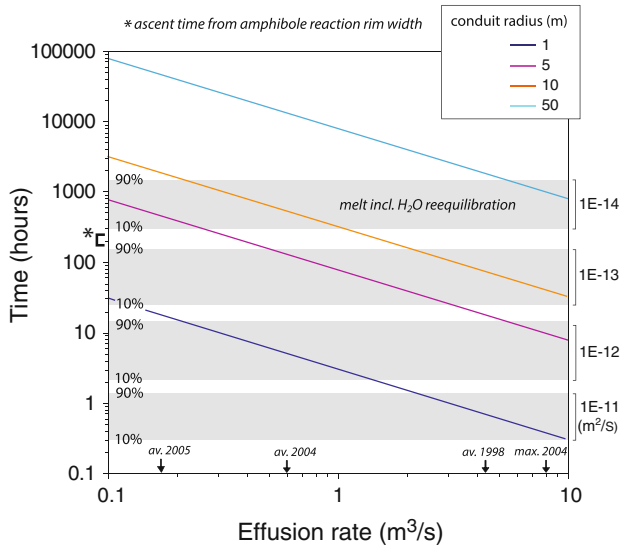

Fig. 9 Timesscales of magma ascent and melt inclusions H_2O diffusive reequilibration in Volcán de Colima subvolcanic magmatic system. *Coloured lines* show the time taken by the magmas to ascend from 4 km as a function of effusion rate and conduit radius. Four kilometres corresponds to the average highest pressure (depth) recorded by the melt inclusions in the 1998–2005 magmas. The times for H_2O diffusive reequilibration of melt inclusions were calculated using the formulation of Qin et al. (1992). *Grey rectangles* represent the range of time for 10–90 % reequilibration of the melt inclusion H_2O contents for different H_2O diffusion coefficient in pyroxenes (values indicated on the right hand axis of the diagram). *Small arrows* on the horizontal axis are the average effusion rates for the different periods of volcanic activity from Table 1. Ascent time estimates based on the hornblendes reaction rim width in the 1998 lava flow are from Luhr (2002)

pyroxenes are in the range 1×10^{-10} to 1×10^{-11} m^2 s^{-1} (Hercule and Ingrin 1999; Stalder and Skogby 2003; Woods et al. 2000). The resulting times of complete H_2O reequilibration are <1.3 h. These times are unrealistically low as all the Colima melt inclusions would be expected to have lost most of their H_2O budget (Fig. 9). Preservation of H_2O contents in melt inclusions from low effusion rate eruptions requires the diffusion coefficients to be $\leq 1 \times 10^{-13}$ m^2 s^{-1}, even in the case of a conduit with a 1 m radius (Fig. 9). Similar diffusion coefficients have been inferred for pyroxenes from mantle xenoliths (Peslier and Luhr 2006) and from pyroxenes in volcanic systems (Wade et al. 2008). The discrepancy between laboratory-based measurement on gem quality minerals and natural systems may reflect the effect of pyroxene composition. For melt inclusion reequilibration, the discrepancy between diffusion coefficient obtained experimentally and inferred from natural samples may also indicate diffusion of molecular H_2O instead of H. Dissociation of H_2O is a prerequisite for H diffusion, but is limited by the ability of the melt to oxidise, which in silicate melt is essentially controlled by the amount of Fe^{2+} (Danyushevsky et al. 2002). For Colima melts, oxidisation of Fe^{2+} correspond at most to 0.3 wt% H_2O. Fe oxidation resulting from H_2O dissociation may be accompanied by precipitation of magnetite. The common occurrence of a small daughter crystal of magnetite in Colima inclusions may indicate H diffusive loss, however, the low proportion of post-entrapment crystallisation of magnetite (<2 %) in the melt inclusions considered here corresponds to small amount of H_2O dissociation (<0.2 %). We not also that there is no correlation between the inferred amount of H_2O loss and FeO contents of the melt inclusions. Diffusion of molecular H_2O through the host pyroxene may, therefore, control post-entrapment H_2O loss from the melt inclusions and is likely to be very much slower than H^+ diffusion.

A better understanding of the processes at play and constraints on the associated diffusion coefficients is essential for quantitative interpretations of H_2O reequilibration of melt inclusions. Nevertheless, preservation of initial H_2O contents in Colima low effusion rate eruptions demonstrates that the diffusion coefficients associated with H_2O loss from the inclusions through the host pyroxenes after entrapment is several orders of magnitudes smaller than experimentally determined H^+ diffusion coefficients in pyroxenes. We note also that the absence of clear textural evidence supporting diffusive loss of H_2O may be an indication that diffusion in melt channels prior to sealing of the inclusions prevails.

Significance of the melt inclusions

The link between degassing and crystallisation

H_2O loss from degassing magmas and/or cooling causes crystallisation in the upper crust. Correlated indices of differentiation and decreasing H_2O contents in melt inclusions are strong indications that dehydration is predominantly controlling crystallisation in vapour-saturated magmatic systems, where the majority of phenocrysts are thought to form (Blundy and Cashman 2005; Johnson et al. 2008; Reubi and Blundy 2009). As discussed above, H_2O contents in some of the melt inclusions are affected by diffusive loss, hence slow-diffusing species and elements like CO_2, S and Cl should be more robust indicators of the degassing trends. However, even when these volatile elements are considered, the melt inclusions from Volcán de Colima do not show a simple relationship between volatile elements and incompatible trace elements that can be used as proxies for indices of differentiation (Fig. 10). CO_2 and S display very broad negative correlations with incompatible trace elements, in agreement with the trend of decreasing H_2O with decreasing MgO (Fig. 8) and indicating that decompression-induced crystallisation occurred. Cl show a broad positive correlation with indices of

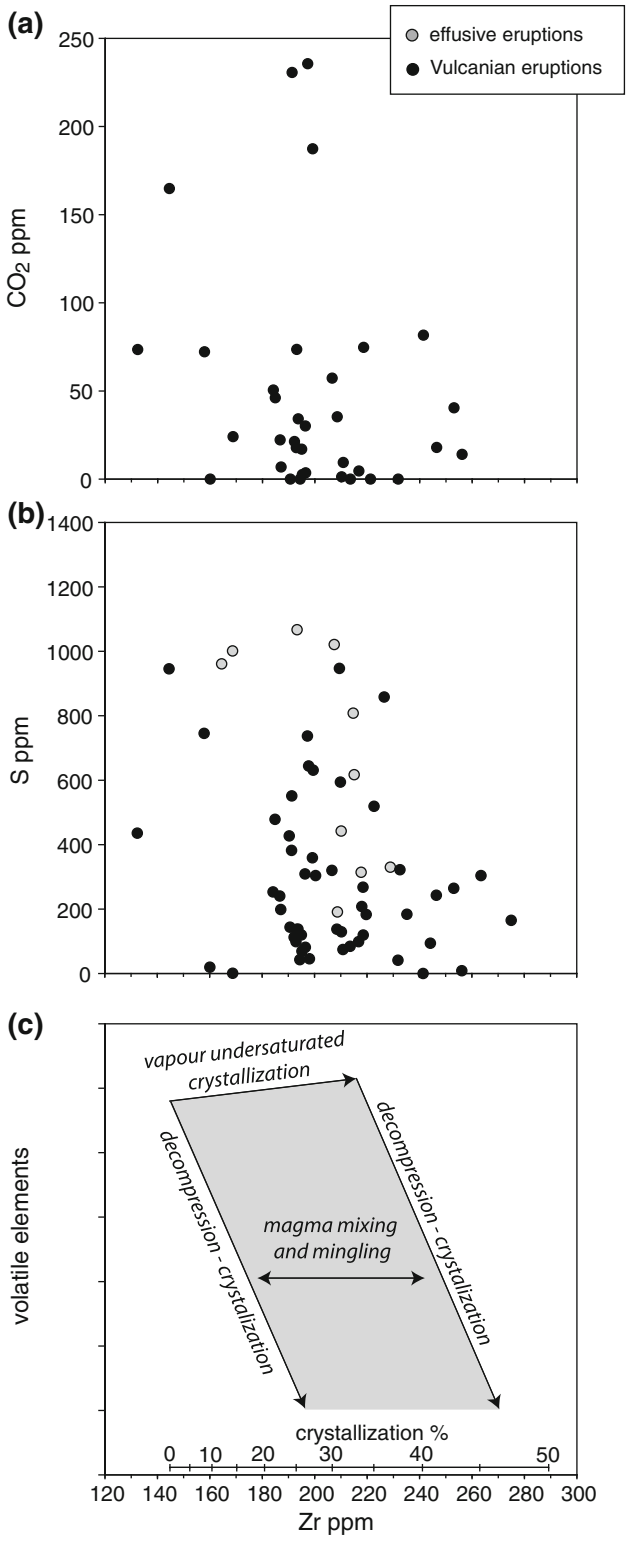

◀**Fig. 10** Melt inclusion CO_2 and S as a function of Zr contents. The schematic plots **c** show the trends anticipated for different crystallisation mechanisms. The *shaded region* denotes the predicted range of melt inclusion compositions generated by a combination of vapour-undersaturated and vapour-saturated crystallisation. Percentages of crystallisation are calculated assuming that Zr is perfectly incompatible in the crystallising assemblage (plagioclase + orthopyroxene + clinopyroxene + Fe–Ti oxides)

differentiation (not shown) consistent with the known negative pressure dependence of Cl solubility in silicate melts (Metrich and Rutherford 1992). The observed spread in the data at Colima may, to some extent, be the result of leakage during decompression of the inclusions. However, the range of incompatible trace element contents obtained for inclusions with relatively high volatile contents suggest that there is a genuine variability in melt compositions. Considering that the melt inclusions show significant spread in major element contents that cannot be fully assigned to post-entrapment crystallisation of the host (Fig. 4), some variability in volatile and incompatible trace element contents is not surprising. This may be a consequence of melt inclusions sampling local and ephemeral heterogeneity in an overall relatively uniform magma batch following a decompression-induced crystallisation trend. The chemical variability is, in this case, an artefact of the melt inclusions with limited significance regarding the magmatic system. Alternatively, this may depict the complexity of the magmatic system and genuine chemical variations between magma batches. In view of the observed spread in volatile, major and trace element contents, and variable amount of H_2O loss experienced by the melt inclusions, we suggest that the melt inclusions chemical variability reflects the evolution of several magma batches. A plausible explanation for the absence of a simple crystallisation–degassing trend involves some variability in mineral assemblages during the crystallisation step that produced the dacitic melts (inferred to occur under vapour-undersaturated conditions in the lower crust), hence producing a range of melt compositions. Upon ascent, these melts reach their volatile-saturated liquidus and follow decompression-induced crystallisation in independent but interconnected reservoirs, likely a network of small sills connected by dykes. Mixing and mingling between ascending magmas result in melt inclusion populations heterogeneous in terms of composition, ascent rate and residence time (i.e. extent of H_2O reequilibration).

Link between the melt inclusion and surface volcano monitoring records

The depths of crystallisation calculated from the pressure of entrapment of the inclusions are in the range 8.4–0 km (below the summit level) with a cluster at depths less than 4 km (Fig. 11). This range closely matches the depths of volcano-tectonic seismic swarms recorded prior to the eruption of the 1998–1999 lava flow (Zobin et al. 2002) (Fig. 11a) and the source location of long-period seismicity

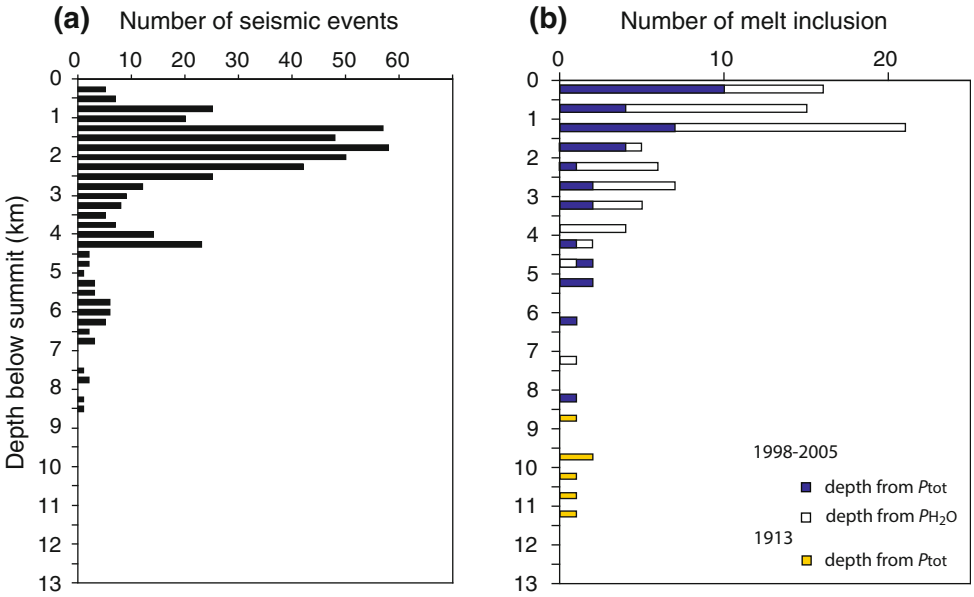

Fig. 11 **a** Histogram showing the depth of volcano-tectonic seismic events recorded in 1997–1998 (data from Zobin et al. 2002). **b** Histogram showing the depths of crystallisation estimated on the basis of entrapment pressure of melt inclusions calculated from dissolved H_2O and CO_2 contents and the solubility model of Papale et al. (2006) and converted to depth according to the method of Pinel and Jaupart (2000), which takes into account the effect of volcanic load. Melt inclusion data for the 1913 Plinian eruption are from Luhr (2006)

recorded by broadband seismic stations between November 2005 and May 2006 (Petrosino et al. 2011). This agreement is an additional indication that, overall, the melt inclusions efficiently record the ascent and crystallisation of the volatile-saturated magma column. The depths of entrapment calculated for the melt inclusions from the 1913 eruption range from 8.8 to 11.1 km, depths at which no seismic signals were recorded in 1998–1999 and 2005–2006. The distinct melt inclusion and crystal populations (Figs. 2, 6) indicate that there is little inheritance of 1913 crystals in the 1998–2005 magmas, consistent with almost complete evisceration of the magma reservoir during the 1913 event. More fundamentally, the temporal match between the melt inclusion and seismic records shows that the melt inclusion population does not provide an integrated record that characterise the range of conditions in the magmatic system during the last hundreds or thousands of years, but effectively depict the current state of the system. Whether this implies that the phenocrysts that host the inclusions formed within a few years to decades of eruption or that the crystals resided at the levels of entrapment of the melt inclusions for significant amount times before being sampled by the current activity remains to be established. But this link demonstrates that the melt inclusions may be used in conjunction with the volcano monitoring signal to interpret subvolcanic magmatic processes, as previously shown at Mount St. Helens (Blundy et al. 2008).

Analysis of the spectral properties of long-period volcanic earthquakes by Petrosino et al. (2011) further identifies a variety of events confined to a small volume lying about 1 km below the crater, which they associated with explosive activity. Decompression experiments performed on Colima ballistic bombs ejected during recent vulcanian eruptions indicate decompression as great as 20 MPa (Lavallee et al.2012), which is equivalent to the lithostatic pressure 1.2 km below the summit. At this pressure, the melts will contain 1.2 wt% H_2O. These observations suggest that the $\sim$1 wt% H_2O melt inclusion reequilibration peak (Fig. 5) could reflect an important physical feature in Colima magmatic system. The viscosity of degassing dacitic melts strongly increase once dissolved H_2O decreases to around 1 wt% (Whittington et al. 2009), magmas are, therefore, expected to stall at a depth corresponding to the equivalent pressure, that is, around 1 km below summit. Preferential reequilibration of the melt inclusions at this level, perhaps via melt tubes connected to the matrix, may be expected, but it also appears to be the source location of volcanic earthquakes associated with vulcanian activity and the lowest pressure inferred for the most explosive events. The pressure corresponding to preferential reequilibration of melt inclusions may, therefore, provide important information on the flow dynamics in the magma conduit. Changes in magma rheology due to H_2O degassing around 20 MPa are likely to be an

important feature controlling the flow dynamics in the conduit and ultimately the explosivity at Colima.

Experimental constraints on the maximum H_2O content of the melt

One of the outstanding questions is why do the 1998–2005 magmas have lower maximum H_2O contents than the 1913 magmas (Fig. 6) and intermediate arc magmas in general. The low maximum H_2O contents could have several causes: (1) the melts feeding the 1998–2005 eruption degassed significantly before crystallising; (2) the parental melts are relatively dry and significant variations in the H_2O-contents of the magmas ascending through the crust occurred over a few decades; (3) the melt inclusions failed to record a significant portion of the degassing–crystallisation path. Moore and Carmichael (1998) and Carmichael (2002) suggested that Volcán de Colima andesitic magmas are generated from degassing and reequilibration during ascent of hydrous parental magmas containing initially at least 6 wt% H_2O that started crystallising in the hornblende ± plagioclase stability field. The H_2O contents of melt inclusions, the presence of euhedral non-resorbed hornblende phenocrysts and the composition of plagioclases in the 1913 magmas support this hypothesis (Luhr 2006; Luhr and Carmichael 1980). Ascent, degassing and reequilibration at low pressure of magmas left in the system after the 1913 eruption could explain the observed shift in H_2O contents from the 1913 to 1998–2005 eruptions. However, as discussed earlier, the 1998–2005 plagioclase compositions support the melt inclusion H_2O contents and indicate that this is not the case. In addition, significant amounts of amphiboles that have become resorbed as the magma crossed the lower stability pressure of hornblende should be observed (Rutherford and Hill 1993). The very small proportion (0–0.5 vol%) of hornblende and the fact that they are systematically resorbed rule out this scenario. We conclude that the 1998–2005 magmas are not degassed equivalent of the 1913 magmas; they crystallised under different P, T or P_{H2O}.

The temperatures given by two-pyroxene thermometer and the highest ilmenite-magnetite temperature, 1,000 ± 30 and 993 °C (Fig. 3), respectively, exceed the maximum temperature of hornblende stability in Colima andesite [between ~930 and 975 °C at 180 MPa depending on the exact melt composition (Fig. 12); (Moore and Carmichael 1998)]. This indicates that the 1998–2005 magmas were hotter than the 1913 magmas and most likely did not start crystallising within the amphibole stability field. Water-saturated phase equilibrium experiments for a spessartite from the Mascota volcanic field (Mexico) that is close in composition to Volcán de Colima andesitic bulk rock compositions (Fig. 4) indicate that, at 1,000 ± 30 °C, these melts may contain up to 4.5–5.5 wt% H_2O on the liquidus (Moore and Carmichael 1998) (Fig. 12). This would imply that the melt contained initially more H_2O than suggested by the melt inclusions, with the implication that the latter failed to record a significant portion of the degassing–crystallisation path [~25 % crystallisation according to the experiments of Moore and Carmichael (1998)]. The plagioclase phenocrysts should, in this case, predominantly show normal zoning and a main population around An_{75-65} (Moore and Carmichael 1998) (Figs. 2a, 12). The main population of plagioclase phenocrysts in the 1998–2005 magmas that show oscillatory zoning has compositions in the range An_{60-40} in the 1998–2005 magmas (Fig. 2a) suggesting that this is not the case.

The composition of the Mascota spessartite, although close to the bulk rock compositions, is more mafic than the composition of the crystallising melt represented by the melt inclusions. Reubi and Blundy (2008) attribute this discrepancy to the entrainment of crystals in a more evolved melt, generating bulk rock compositions that are distinctly more mafic than any true liquids ever present in the system. In this case, experiments on a starting composition that matches the bulk rock are of questionable value in understanding melt evolution. Further insights may be glaned from looking at experiments performed on starting materials that more closely represent the melt that entrained the crystal cargo. Vapour-saturated experiments on a Mount St. Helens dacite that is closer in composition to the Colima melt inclusions (Fig. 4), produced plagioclases with composition similar to the main population in Colima 1998–2005 magmas from melts with 2.8–4.5 wt% H_2O on the liquidus at 1,000 ± 30 °C (Rutherford et al. 1985) (Fig. 12b). In that case, the H_2O contents given by our melt inclusions could record the H_2O content of the melt at or near the liquidus at the range of estimated temperature. The maximum amount of H_2O dissolved in the melt at the onset of crystallisation (and that can possibly be recorded by the melt inclusions) is, in this case, dictated by the slope of the liquidus in temperature and pressure space, and the melt could have degassed significantly before intersecting the vapour-saturated liquidus (cf. Annen et al. 2006). The relatively low maximal H_2O contents in Colima 1998–2005 magmas are most certainly a consequence of their relatively high temperatures leading to degassing before the onset of vapour-saturated crystallisation. We note that the Mascota experiments and those from Mount St. Helens used to define the liquidus are for pure H_2O vapour $\left(X_{H_2O(vap)} = 1\right)$, when Volcán de Colima least-degassed melt inclusions equilibrated with vapours containing CO_2 $\left(X_{H_2O(vap)} \approx 0.75\right)$. Reduced $X_{H2O(vap)}$ will elevate the liquidus temperature compared to

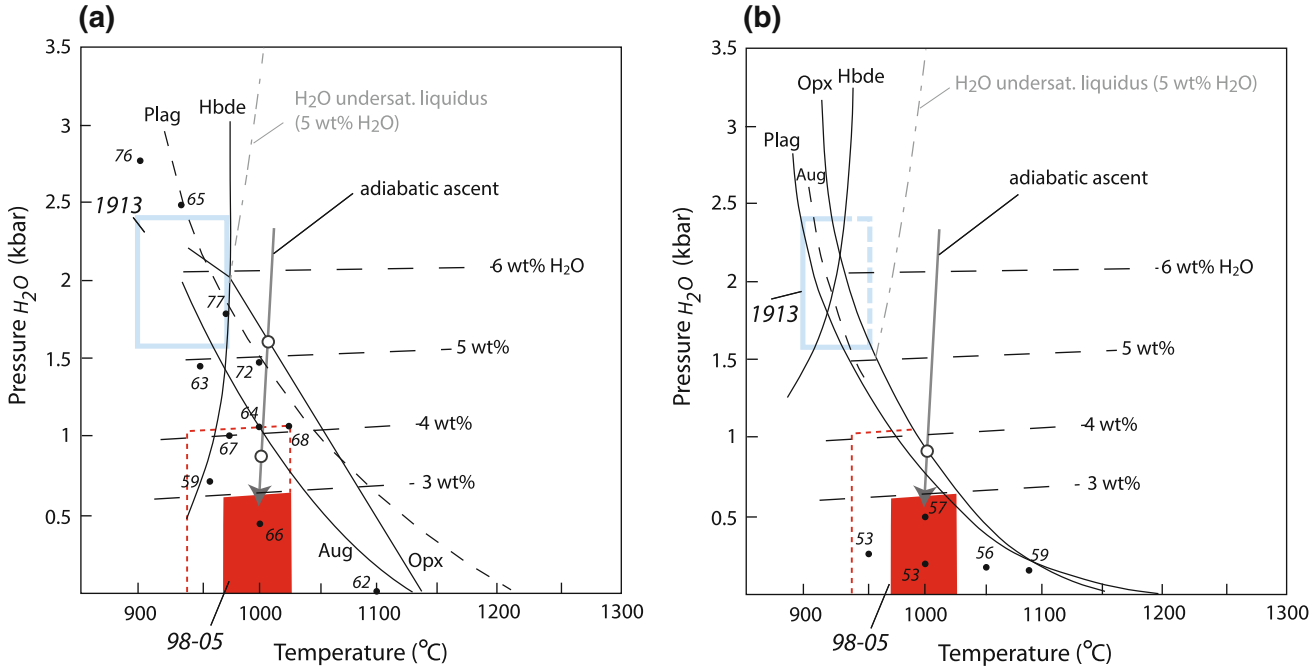

Fig. 12 H_2O-saturated pressure–temperature phase diagram for andesitic to dacitic compositions. **a** Phase diagram for a Mascota andesite in equilibrium with pure H_2O vapour $\left(X_{H_2O(vap)} = 1\right)$; data from Moore and Carmichael (1998). **b** Phase diagram for a Mount St Helens dacite in equilibrium with pure H_2O vapour $\left(X_{H_2O(vap)} = 1\right)$; data from Rutherford et al. (1985). The *red areas* marked 98-05 represent the predominant conditions inferred for Volcán de Colima 1998–2005 magmas on the basis of the melt inclusion composition (83 out of 84 analyses) and two pyroxenes thermometer data. The *red dashed* line represents the conditions of crystallisation taking into account the complete melt inclusion population [a single analyses with 4.1 wt% H_2O (Fig. 5)], the reported errors for the two pyroxenes thermometer (2 out of the 15 pairs used for thermometry have *error bars* extending below 960 °C) and the lowest temperature given by the ilmenite–magnetite thermometer. The *blue area* marked 1913 represents the conditions prior to the 1913 Plinian eruption estimated on the basis of melt inclusion composition, two-pyroxene thermometry and amphibole-plagioclase thermometry data (Luhr 2002; Savov et al. 2008; our unpublished data). Small numbers next to the *black dots* give the An% of plagioclase in Moore and Carmichael (1998) and Rutherford et al. (1985) [These experiments are in equilibrium with H_2O–CO_2 vapour $\left(X_{H_2O(vap)} = 0.1 - 0.5\right)$] experiments, respectively. Isopleths of water concentration are calculated for the average melt inclusion composition (67.8 wt% SiO_2) using the solubility model of Papale et al. (2006). H_2O-undersaturated liquidus for a silicic andesite melt with 5 wt% H_2O from Annen et al. (2006). During adiabatic ascent, a dacitic melt similar in composition to the melt inclusions and at 1,000 °C (represented by the *grey arrows* in **b**) will not start crystallising until it reaches the vapour-saturated liquidus. For a melt in equilibrium with pure H_2O vapour, this corresponds to ~4 wt% H_2O at the liquidus. Any H_2O in excess of this value will degas prior to crystallisation and will not be recorded by the melt inclusions. The melt inclusions H_2O contents (0.1–4.1 wt%) and the composition of plagioclase phenocrysts (An_{60-40}) in 1998–2005 magmas are compatible with a decompression-crystallisation trend from $PH_2O = 1$ kbar at ~1,000 °C, that is, the temperatures estimated using two-pyroxene thermometry

the H_2O-saturated case, which results in a simple offset between PH_2O and Ptot on the vertical axis in Fig. 12. This will have negligible impact on our proposed magma ascent and crystallisation scenario.

The arguments presented above suggest that the bulk of crystallisation occurred at low PH_2O. High plagioclase An% may reflect crystallisation in more mafic melt or increase in melt H_2O content. Consequently, the presence of normally zoned Ca-rich plagioclases (to An_{82}) (Fig. 2) in Colima magmas could potentially record an earlier phase of crystallisation at high P_{H2O} (Carmichael 2002; Moore and Carmichael 1998). Trace elements for which the partitioning between crystal and melt is known can be used to trace variations in melt composition and decipher the parameters controlling the plagioclase An%. The positive correlation between the plagioclase An% and calculated melt composition (Fig. 2b) indicates that the Ca-rich plagioclases crystallised from Sr-rich mafic melts. Therefore, melt composition rather than P_{H2O} is the primary control on the plagioclase composition in these magmas. Disaggregation of gabbroic fragments is likely to be the source of these An-rich crystals (Reubi and Blundy 2008). Amongst the crystal analysed, only one crystal shows high An% at a given melt Sr content (Fig. 2b). This crystal most likely formed at higher PH_2O than the other plagioclases. It was probably entrained from cumulates that also comprised the rare resorbed amphiboles observed in the 1998–2005 magmas. These possibly represent rare residual crystals left in the magmatic system after the 1913 eruption.

In summary, the melt inclusions and the petrology indicate that the 1998–2005 magmas had low H_2O contents from the onset of crystallisation. This may indicate that these magmas were produced by differentiation of relatively dry basaltic melts or by differentiation of vapour-saturated hydrous basaltic melt at low pressure. Alternatively, this may reflect attainment of volatile saturation at temperatures above the vapour-saturated liquidus. The 1998–2005 magmas may initially have had 6 wt% H_2O like the 1913 magmas. At temperatures that exceed the amphibole stability field, they will attain H_2O saturation at a temperature above the liquidus (Fig. 12b). Degassing would, therefore, not be accompanied by crystallisation until the melt intersects the vapour-saturated liquidus, and significant amount of water (and CO_2) may be lost before crystallisation of the phenocrysts and sealing of the melt inclusions. We believe that this process is controlling the relatively low maximal H_2O contents in Colima 1998–2005 magmas.

Conclusions

Pyroxene-hosted melt inclusions from Volcán de Colima 1998–2005 magmas have experienced variable extent of H_2O reequilibration, ranging from negligible up to 2 wt% H_2O loss. H_2O loss is, nevertheless, a second-order process and the melt inclusions effectively record the range of H_2O contents of the crystallising melts when the complete population is considered. Preservation of H_2O contents close to their entrapment values in some melt inclusions from effusive eruptions with low effusion rates requires the diffusion coefficients associated with post-entrapment H_2O diffusion through the host crystal ($\leq 1 \times 10^{-13}$ m^2 s^{-1}) to be at least several orders of magnitude smaller than experimentally determined H^+ diffusion in pyroxenes. These low post-entrapment diffusion coefficients and the absence of textural evidences supporting post-entrapment H_2O loss suggest that, in the case of partially reequilibrated melt inclusions, diffusion may occur principally in melt channels prior to sealing of the inclusions.

Volcán de Colima melt inclusions do not show a simple relationship between crystallisation and degassing, although the broad inverse correlations between indices of differentiation and volatile contents in the melts indicate that decompression-induced crystallisation predominates. We suggest that this absence of a simple relationship results from a combination of early, vapour-undersaturated crystallisation steps and subsequent volatile-saturated crystallisation of separate magma batches that are brought together upon eruption.

The depths recorded by the 1998–2005 melt inclusions correspond to the depths of seismic sources recorded in 1997–1998 and 2005–2006, when the melt inclusions from the 1913 eruption record distinctively higher pressures corresponding to depths in the system without current seismicity. This temporal link is an additional indication that the melt inclusion population effectively documents crystallisation and degassing of the magmas in the subvolcanic system prior to eruption and not a record that integrates hundreds of years of activity. Consequently, the melt inclusions may be used in conjunction with the volcano monitoring signal to interpret pre-eruptive subvolcanic magmatic processes.

Although the melt inclusions effectively record the evolution of the magmas during degassing and crystallisation, their ability to document the maximal H_2O contents of the melt is questionable. In the Colima case, we suggest that the moderate H_2O contents indicated by the melt inclusions are a consequence of the fact these magmas crystallised at high temperature, under vapour-saturated conditions and outside the amphibole stability field. At these conditions, the amount of volatiles dissolved in the melt at the onset of crystallisation is controlled by the slope of the liquidus in P–T space and volatile-rich magmas ascending along the adiabat may reach vapour saturation at depths greater than those at which they intersect the vapour-saturated liquidus. Significant amounts of volatiles may consequently be lost before crystallisation and sealing of the melt inclusions. This situation will prevail for all H_2O-rich magmas at temperatures exceeding the amphibole stability field (950–1,000 °C depending on the melt composition) and is, therefore, expected to control the melt inclusion maximal H_2O contents in hydrous mafic magmas.

Acknowledgments This work was supported by a Swiss NSF Ambizione fellowship to OR. JB acknowledges support from ERC Advanced Grant "CRITMAG". NV acknowledges assistance from the Universidad de Colima FRABA 768/11 and 639/09. We are grateful to Richard Hinton (Ion Microprobe Facility, University of Edinburgh) for assistance with ion microprobe analysis. The comments of 5 anonymous reviewers helped to improve the manuscript.

References

Andersen DJ, Lindsley DH, Davidson PM (1993) Quilf: a Pascal Program to Assess Equilibria among Fe-Mg-Mn-Ti oxides, pyroxenes, olivine, and quartz. Comput Geosci 19:1333–1350

Annen C, Blundy JD, Sparks RSJ (2006) The genesis of intermediate and silicic magmas in deep crustal hot zones. J Petrol 47:505–539

Atlas ZD, Dixon JE, Sen G, Finny M, Lillian A, Pozzo MD (2006) Melt inclusions from Volcan Popocatepetl and Volcan de Colima, Mexico: melt evolution due to vapor-saturated crystallization during. J Volcanol Geotherm Res 153:221–240

Blundy J, Cashman K (2005) Rapid decompression-driven crystallization recorded by melt inclusions from mount st. Helens volcano Geology 33:793–796

Blundy JD, Wood BJ (1991) Crystal-chemical controls on the partitioning of Sr and Ba between plagioclase feldspar, silicate melts, and hydrothermal solutions. Geochim Cosmochimica Acta 55:193–209

Blundy J, Cashman K, Berlo K (2008) Evolving magma storage conditions beneath mount st. Helens inferred from chemical variations in melt inclusions from the 1980–1986 and current eruptions. USGS Prof Paper 1750:755–790

Blundy J, Cashman K, Rust A, Witham F (2010) A case for CO_2-rich arc magmas. Earth Planet Sci 290:289–301

Bouvet de Maisonneuve C, Dungan MA, Bachmann O, Burgisser A (2012) Insights into shallow magma storage and crystallization at Volcan Llaima (Andean Southern Volcanic Zone, Chile). J Volcanol Geotherm Res 211:76–91

Breton M, Ramirez JJ, Navarro C (2002) Summary of the historical eruptive activity of Volcan de Colima, Mexico 1519–2000. J Volcanol Geotherm Res 117:21–46

Carmichael ISE (2002) The andesite aqueduct: perspectives on the evolution of intermediate magmatism in west-central (105–99 degrees W) Mexico. Contrib Mineral Petrol 143:641–663

Collins SJ, Pyle DM, Maclennan J (2009) Melt inclusions track pre-eruption storage and dehydration of magmas at Etna. Geology 37:571–574

Cooper KM, Reid M (2008) Uranium-series crystal ages. Rev Mineral Geochem 69:479–544

Danyushevsky LV, McNeill AW, Sobolev AV (2002) Experimental and petrological studies of melt inclusions in phenocrysts from mantle-derived magmas: an overview of techniques, advantages and complications. Chem Geol 183:5–24

Ghiorso M, Evans B (2008) Thermodynamics of rhombohedral oxide solid solutions and a revision of the Fe-Ti two-oxide geothermometer and oxygen-barometer. Am J Sci 308:957–1039

Gonnermann HM, Manga M (2005) Nonequilibrium magma degassing: results from modeling of the ca.1340 AD eruption of mono craters. Calif Earth Planet Sci 238:1–16

Hauri E (2002) SIMS analysis of volatiles in silicate glasses, 2: isotopes and abundances in Hawaiian melt inclusions. Chem Geol 183:115–141

Hercule S, Ingrin J (1999) Hydrogen in diopside: diffusion, kinetics of extraction-incorporation, and solubility. Am Mineral 84:1577–1587

Humphreys MCS, Blundy JD, Sparks RSJ (2006) Magma evolution and open-system processes at Shiveluch Volcano: insights from phenocryst zoning. J Petrol 47:2303–2334

Humphreys MCS, Blundy JD, Sparks RSJ (2008a) Shallow-level decompression crystallisation and deep magma supply at Shiveluch Volcano. Contrib Mineral Petrol 155:45–61

Humphreys MCS, Menand T, Blundy JD, Klimm K (2008b) Magma ascent rates in explosive eruptions: constraints from H2O diffusion in melt inclusions. Earth Planet Sci 270:25–40

Johnson ER, Wallace PJ, Cashman KV, Granados HD, Kent AJR (2008) Magmatic volatile contents and degassing-induced crystallization at Volcán Jorullo, Mexico: implications for melt evolution and the plumbing systems of monogenetic volcanoes. Earth Planet Sci 269:477–486

Johnson ER, Wallace PJ, Cashman KV, Delgado Granados H (2010) Degassing of volatiles (H_2O, CO_2, S, Cl) during ascent, crystallization, and eruption at mafic monogenetic volcanoes in central Mexico. J Volcanol Geotherm Res 197:225–238

Kelley KA, Plank T, Newman S, Stolper EM, Grove TL, Parman S, Hauri EH (2010) Mantle melting as a function of water content beneath the mariana arc. J Petrol 51:1711–1738

Koleszar AM, Kent AJR, Wallace PJ, Scott WE (2012) Controls on long-term low explosivity at andesitic arc volcanoes: insights from Mount Hood, Oregon. J Volcanol Geotherm Res 219:1–14

Kress VC, Carmichael ISE (1991) The compressibility of silicate liquids containing Fe_2o_3 and the effect of composition, temperature, oxygen fugacity and pressure on their Redox States. Contrib Mineral Petrol 108:82–92

Lange RA, Frey HM, Hector J (2009) A thermodynamic model for the plagioclase-liquid hygrometer/thermometer. Am Mineral 94:494–506

Lavallee Y, Varley NR, Alatorre-Ibargueengoitia MA, Hess KU, Kueppers U, Mueller S, Richard D, Scheu B, Spieler O, Dingwell DB (2012) Magmatic architecture of dome-building eruptions at Volcan de Colima, Mexico. B Volcanol 74:249–260

Lloyd A, Plank T, Ruprecht P, Hauri E, Rose W (2012) Volatile loss from melt inclusions in pyroclasts of differing sizes. Contrib Mineral Petrol. doi:10.1007/s00410-012-0800-2

Lowenstern JB (2003) Melt inclusions come of age: volatiles, volcanoes and Sorby's legacy. In: De Vivo B, Bodnar RJ (eds) Melt inclusions in volcanic systems: methods, applications and problems. Elsevier, Amsterdam, pp 1–21

Luhr JF (2002) Petrology and geochemistry of the 1991 and 1998–1999 lava flows from Volcan de Colima, Mexico: implications for the end of the current eruptive cycle. J Volcanol Geotherm Res 117:169–194

Luhr JF (2006) The 1913 VEI-4 Plinian eruption of Volcan de Colima (Mexico): tephrochronology, petrology and plume modeling. AGU fall meeting 87:V43B-1786

Luhr JF, Carmichael ISE (1980) Colima Volcanic complex, Mexico.1. post-caldera andesites from Volcan Colima. Contrib Mineral Petrol 71:343–372

Luhr JF, Carmichael ISE (1990) Petrological monitoring of cyclical eruptive activity at Volcan-Colima, Mexico. J Volcanol Geotherm Res 42:235–260

Luhr JF, Prestegaard KL (1988) Caldera formation at Volcano Colima, Mexico, by a large Holocene Volcanic Debris avalanche. J Volcanol Geotherm Res 35:335–348

Massare D, Metrich N, Clocchiatti R (2002) High-temperature experiments on silicate melt inclusions in olivine at 1 atm: inference on temperatures of homogenization and H2O concentrations. Chem Geol 183:87–98

Melnik O, Sparks RSJ (1999) Nonlinear dynamics of lava dome extrusion. Nature 402:37–41

Metrich N, Rutherford MJ (1992) Experimental-study of chlorine behavior in hydrous silicic Melts. Geochim Cosmochimica Acta 56:607–616

Mollo S, Putirka K, Iezzi G, Del Gaudio P, Scarlato P (2011) Plagioclase-melt (dis) equilibrium due to cooling dynamics: implications for thermometry, barometry and hygrometry. Lithos 125(1–2):221–235

Moore G, Carmichael ISE (1998) The hydrous phase equilibria (to 3 kbar) of an andesite and basaltic andesite from western Mexico: constraints on water content and conditions of phenocryst growth. Contrib Mineral Petrol 130:304–319

Mora JC, Macias JL, Saucedo R, Orlando A, Manetti P, Vaselli O (2002) Petrology of the 1998–2000 products of Volcan de Colima, Mexico. J Volcanol Geotherm Res 117:195–212

Newman S, Lowenstern JB (2002) Volatilecalc: a silicate melt-H_2O–CO_2 solution model written in Visual Basic for excel. Comp Geosc 28:597–604

O'Leary JA, Gaetani GA, Hauri EH (2010) The effect of tetrahedral Al(3+) on the partitioning of water between clinopyroxene and silicate melt. Earth Planet Sci 297:111–120

Papale P, Moretti R, Barbato D (2006) The compositional dependence of the saturation surface of $H_2O + CO_2$ fluids in silicate melts. Chem Geol 229:78–95

Peslier AH, Luhr JF (2006) Hydrogen loss from olivines in mantle xenoliths from Simcoe (USA) and Mexico: mafic alkalic magma

ascent rates and water budget of the sub-continental lithosphere. Earth Planet Sci 242:302–319
Petrosino S, Cusano P, La Rocca M, Galluzzo M, Orozco-Rojas J, Bretón M, Ibáñez J, Del Pezzo E (2011) Source location of long period seismicity at Volcàn de Colima, México. B Volcanol 73:887–898
Pinel V, Jaupart C (2000) The effect of edifice load on magma ascent beneath a volcano. Phil Trans Royal Soc Lond 358:1515–1532
Portnyagin M, Almeev R, Matveev S, Holtz F (2008) Experimental evidence for rapid water exchange between melt inclusions in olivine and host magma. Earth Planet Sci 272:541–552
Putirka KD (2005) Igneous thermometers and barometers based on plagioclase plus liquid equilibria: tests of some existing models and new calibrations. Am Mineral 90:336–346
Putirka KD (2008) Thermometers and barometers for volcanic systems. Rev Mineral Geochem 69:61–120
Qin ZW, Lu FQ, Anderson AT (1992) Diffusive reequilibration of melt and fluid inclusions. Am Mineral 77:565–576
Reid M (2003) Timescales of magma transfer and storage in the crust. Treatise Geochem 3:167–193
Reubi O, Blundy J (2008) Assimilation of plutonic roots, formation of high-K exotic melt inclusions and genesis of andesitic magmas at Volcán de Colima, Mexico. J Petrol 49:2221–2243
Reubi O, Blundy J (2009) A dearth of intermediate melts at subduction zone volcanoes and the petrogenesis of arc andesites. Nature 461:1269–1273
Roggensack K (2001) Unraveling the 1974 eruption of Fuego volcano (Guatemala) with small crystals and their young melt inclusions. Geology 29:911–914
Roggensack K, Hervig RL, McKnight SB, Williams SN (1997) Explosive basaltic volcanism from Cerro Negro volcano: influence of volatiles on eruptive style. Science 277:1639–1642
Rust AC, Cashman KV, Wallace PJ (2004) Magma degassing buffered by vapor flow through brecciated conduit margins. Geology 32:349–352
Rutherford MJ, Hill PM (1993) Magma ascent rate from amphibole breakdown: an experimental study applied to the 1980–1986 Mount St Helens eruptions. J Geophys Res 98:19667–19685
Rutherford MJ, Sigurdsson H, Carey S, Davis AM (1985) The May 18, 1980, eruption of mount st. Helens 1. Melt composition and experimental phase equilibria. J Geophys Res 90:2929–2947
Savov IP, Luhr JF, Navarro-Ochoa C (2008) Petrology and geochemistry of lava and ash erupted from Volcan Colima, Mexico, during 1998–2005. J Volcanol Geotherm Res 174:241–256
Schmitt AK (2001) Gas-saturated crystallization and degassing in large-volume, crystal-rich dacitic magmas from the Altiplano-Puna, northern Chile. J Geophys Res 106:30561–30578
Severs MJ, Azbej T, Thomas JB, Mandeville CW, Bodnar RJ (2007) Experimental determination of H2O loss from melt inclusions during laboratory heating: evidence from Raman spectroscopy. Chem Geol 237:358–371
Sisson TW, Grove TL (1993) Experimental investigations of the role of H_2O in calc-alkaline differentiation and subduction zone magmatism. Contrib Mineral Petrol 113:143–166
Sisson TW, Layne GD (1993) H_2O in Basalt and Basaltic Andesite Glass Inclusions from 4 Subduction-Related Volcanos. Earth Planet Sci 117:619–635
Sparks RSJ (1997) Causes and consequences of pressurisation in lava dome eruptions. Earth Planet Sci Lett 150:177–189
Spilliaert N, Allard P, Metrich N, Sobolev AV (2006) Melt inclusion record of the conditions of ascent, degassing, and extrusion of volatile-rich alkali basalt during the powerful 2002 flank eruption of Mount Etna (Italy). J Geophys Res. doi: 10.1029/2005JB003934
Stalder R, Skogby H (2003) Hydrogen diffusion in natural and synthetic orthopyroxene. Phys Chem Minerals 30:12–19
Wade JA, Plank T, Hauri EH, Kelley KA, Roggensack K, Zimmer M (2008) Prediction of magmatic water contents via measurement of H_2O in clinopyroxene phenocrysts. Geology 36:799–802
Wallace PJ (2005) Volatiles in subduction zone magmas: concentrations and fluxes based on melt inclusion and volcanic gas data. J Volcanol Geotherm Res 140:217–240
Wallace PJ, Anderson AT, Davis AM (1999) Gradients in H2O, CO2, and exsolved gas in a large-volume silicic magma system: interpreting the record preserved in melt inclusions from the Bishop Tuff. J Geophys Res 104:20097–20122
Whittington A, Hellwig B, Behrens H, Joachim B, Stechern A, Vetere F (2009) The viscosity of hydrous dacitic liquids: implications for the rheology of evolving silicic magmas. B Volcanol 71:185–199
Woods SC, Mackwell S, Dyar D (2000) Hydrogen in diopside: diffusion profiles. Am Mineral 85:480–487
Zobin VM, Amezcua MG, Davila GAR, Dominguez T, Chacon JCC, Alvarez JMC (2002) Comparative characteristics of the 1997–1998 seismic swarms preceding the November 1998 eruption of Volcan de Colima, Mexico. J Volcanol Geotherm Res 117:47–60